Computational Economics
https://doi.org/10.1007/s10614-023-10500-5

An Efficient Numerical Method Based on Exponential B-splines for a Time-Fractional Black–Scholes Equation Governing European Options

Anshima Singh[1] · **Sunil Kumar**[1]

Accepted: 16 October 2023

Abstract
In this paper a time-fractional Black–Scholes model (TFBSM) is considered to study the price change of the underlying fractal transmission system. We develop and analyze a numerical method to solve the TFBSM governing European options. The numerical method combines the exponential B-spline collocation to discretize in space and a finite difference method to discretize in time. The method is shown to be unconditionally stable using von-Neumann analysis. Also, the method is proved to be convergent of order two in space and $2-\mu$ is time, where μ is order of the fractional derivative. We implement the method on various numerical examples in order to illustrate the accuracy of the method, and validation of the theoretical findings. In addition, as an application, the method is used to price several different European options such as the European call option, European put option, and European double barrier knock-out call option. Moreover, the classical Black–Scholes model is also incorporated into our numerical study to validate the competence of our method in handling not only fractional problems, but also classical ones with favorable results.

Keywords Time-fractional · Black–Scholes model · European option · Exponential B-splines · Collocation method

Mathematics Subject Classification 65M70 · 65M15 · 65M12

✉ Sunil Kumar
skumar.mat@iitbhu.ac.in

Anshima Singh
anshima.singh.rs.mat18@itbhu.ac.in

[1] Department of Mathematical Sciences, Indian Institute of Technology (BHU), Varanasi, India

Published online: 08 November 2023

1 Introduction

In the market of finance, investors need to minimize and control risks. By market risks, we mean the chances of the deficit because of those aspects that impact the inclusive performance of the markets. Investors can manage these types of risks by investing in significant instruments that remove the risk of price volatility. Such instruments are known as financial derivatives. The value of a financial derivative depends on the functioning of the underlying asset. Among many financial derivatives, an option is one of the most well-known and important derivatives, so pricing an option is a significant problem both in practice and in theory. In 1973, (Black and Scuholes 2019) and (Merton 1973) had proposed the Black–Scholes model, which gives an accurate delineation of the behavior of the underlying asset. Black–Scholes model is a second-order parabolic partial differential equation with respect to stock price and time, that governs the European option value on a stock, whose price pursues the geometric Brownian motion with fixed interest rate and constant volatality. Since the Black–Scholes model is simple and effective to model option value, it led to a revolution in the financial market over the past several decades. The classical Black–Scholes model is given by Rodrigo and Mamon (2006); Bohner and Zheng (2009)

$$\begin{aligned}&\frac{\partial \mathcal{V}(\xi,\tau)}{\partial \tau}+\frac{\sigma^2\xi^2}{2}\frac{\partial^2 \mathcal{V}(\xi,\tau)}{\partial \xi^2}+(r_f-D_Y)\xi\frac{\partial \mathcal{V}(\xi,\tau)}{\partial \xi}\\&-r_f\mathcal{V}(\xi,\tau)=0,\ (\xi,\tau)\in\mathbb{R}^+\times(0,\widetilde{T}),\end{aligned}\tag{1}$$

with the terminal condition

$$\mathcal{V}(\xi,\widetilde{T})=\max(\xi_{\widetilde{T}}-\widetilde{K},0),\quad \xi_{\widetilde{T}}\geq 0,\tag{2}$$

where $\mathcal{V}(\xi,\tau)$ denotes the value of a European option price. Here, $\sigma(\xi,\tau)$, $r_f(\tau)$, $D_Y(\tau)$, $\widetilde{T}$, $\widetilde{K}$, and τ represent the volatility of the returns from the holding stock price ξ, the risk free rate, the dividend yield, the expiry time, the exercise price, and the current time respectively. Several approaches have been proposed in the literature to obtain a solution to the classical Black–Scholes model (Amster et al. 2002, 2003; Company et al. 2008, 2009; Bohner and Zheng 2009; Cen and Le 2011). Due to the unrealistic assumptions used in the Black–Scholes model, it has some drawbacks, so it cannot explain a few existing phenomena such as stock price volatility, a short time boom in the financial market. (Carr and Wu 2003), etc.

Fractional integrals and fractional derivatives are non-local, so they are a useful tool to desribe memory. Fractional differential equations have become a powerful tool for studying fractal dynamics and fractal geometry. The fractional calculus has had a massive impact on financial theory, as the fractional Black Scholes model can deal with most of the shortcomings of the classical Black Scholes model. Wyss was the first researcher to introduce the time-fractional Black Scholes model for pricing a European call option (Wyss 2000). To deal with the problem of short time jumps in the financial market, Cartea and del-Castillo-Negrete (Cartea and

Del-Castillo-Negrete 2007) developed the space fractional Black–Scholes model to price exotic options. Jumarie (Jumarie 2008, 2010) applied Itô's lemma and the fractional-order Taylor's series method to obtain the time-space fractional Black–Scholes model. He studied the dynamics of the stock exchange and also considered Merton's optimal portfolio to provide new results. (Liang et al. 2010) derived a bi-fractional Black–Merton–Scholes model. With growth of applications of fractional models in financial field, researchers have shown interest in solving them analytically (Chen et al. 2015; Prathumwan and Trachoo 2020; Ghandehari and Ranjbar 2014; Edeki et al. 2017; Fall et al. 2019) and numerically (Zhang et al. 2016a; De Staelen and Hendy 2017; Song and Wang 2013; Koleva and Vulkov 2017; Golbabai and Mohebianfar 2017; Hariharan et al. 2013; Mesgarani et al. 2021; An et al. 2021; Akram et al. 2022; Chen et al. 2015).

Spline functions are prevalent in mathematics, computer science, engineering, etc. (Rao et al. 2010; Gupta and Kadalbajoo 2016; Kadalbajoo and Gupta 2010; Singh et al. 2023; Kadalbajoo and Gupta 2009; Kadalbajoo et al. 2008; Singh et al. 2023). One common issue with piecewise cubic polynomial spline interpolation is the presence of undesirable inflection points. The exponential spline interpolation method, which extends the concept of cubic splines, serves as a solution to mitigate and avoid these undesired inflection points. Pruess (1979, 1976) demonstrated that exponential splines have the remarkable ability to generate co-monotone and co-convex interpolants, thereby addressing the issue of inflection points. Extensive research on exponential splines was carried out by Pruess (1979), De Boor and De Boor (1978), and McCartin (1991). In addition, McCartin's findings showcased the ability of exponential splines to be represented by a B-spline basis, thereby making them a versatile choice for approximating solutions in differential equation problems of various classes (see Rao and Kumar 2008; Ravi Kanth and Garg 2022, 2021; Singh and Kumar 2023 and the references therein).

To the best of our knowledge, there is no result in the literature on the collocation method based on exponential B-spline functions for the time–fractional Black–Scholes model. So, we propose an effective collocation technique to solve the time–fractional Black–Scholes problem numerically. To achieve this we use exponential B-spline functions to discretize the space derivative and apply a finite difference method to discretize the Caputo fractional derivative. It is proved that the method is unconditionally stable by means of von Neumann analysis. Further, it is shown that the proposed method is convergent of order $O(h_x^2, h_t^{2-\mu})$, where h_t and h_x represent mesh spacing in the time and space directions, respectively. We perform several numerical experiments to validate the theoretical findings. We use the proposed method to price three European options governed by a TFBSM, namely the European call option, the European put option, and the European double barrier knock-out call option. In addition, we examine how the order of time-fractional derivative affects the option price.

The remaining paper is as structured follows. Section 2 describes the model problem. Section 3 is devoted to the proposed numerical method. The stability and convergence of the method are discussed in Sects. 4 and 5 respectively. To validate our

theoretical findings, several numerical examples are considered in Sect. 6. Finally, the paper is concluded in Sect. 7.

2 The Model Problem

Consider the following time-fractional Black–Scholes model (TFBSM) that expresses the option price problem

$$\frac{\partial^{\mu}\mathscr{V}(\xi,\tau)}{\partial\tau^{\mu}}+\frac{\sigma^2\xi^2}{2}\frac{\partial^2\mathscr{V}(\xi,\tau)}{\partial\xi^2}+r_f\xi\frac{\partial\mathscr{V}(\xi,\tau)}{\partial\xi}-r_f\mathscr{V}(\xi,\tau)=0,\quad(\xi,\tau)\in\mathbb{R}^+\times(0,\widetilde{T}),\tag{3}$$

with

$$\begin{cases}\mathscr{V}(\xi,\widetilde{T})=\phi(\xi),\\ \mathscr{V}(0,\tau)=\widetilde{\mathscr{H}}(\tau),\\ \mathscr{V}(\infty,\tau)=\widetilde{\mathscr{G}}(\tau),\end{cases}\tag{4}$$

where $0<\mu\leq 1$ and all other notations are same as defined for problem (1). Further, the modified Riemann–Liouville fractional time derivative is defined by Podlubny (1998)

$$\frac{\partial^{\mu}\mathscr{V}(\xi,\tau)}{\partial\tau^{\mu}}=\begin{cases}\frac{1}{\Gamma(1-\mu)}\frac{d}{d\tau}\int_{\tau}^{\widetilde{T}}\frac{\mathscr{V}(\xi,\nu)-\mathscr{V}(\xi,\widetilde{T})}{(\nu-\tau)^{\mu}}d\nu, & 0<\mu<1,\\ \frac{\partial\mathscr{V}}{\partial\tau} & \mu=1.\end{cases}\tag{5}$$

When $\mu=1$, the model (3)-(4) converts to the classical Black–Scholes model (1)-(2).

We consider the transformation $\tau=\widetilde{T}-t$, for $0<\mu<1$, and proceed as follows

$$\begin{aligned}\frac{\partial^{\mu}\mathscr{V}(\xi,\tau)}{\partial\tau^{\mu}}&=\frac{1}{\Gamma(1-\mu)}\frac{d}{d\tau}\int_{\tau}^{\widetilde{T}}\frac{\mathscr{V}(\xi,\nu)-\mathscr{V}(\xi,\widetilde{T})}{(\nu-\tau)^{\mu}}d\nu\\ &=\frac{-1}{\Gamma(1-\mu)}\frac{d}{dt}\int_{\widetilde{T}-t}^{\widetilde{T}}\frac{\mathscr{V}(\xi,\nu)-\mathscr{V}(\xi,\widetilde{T})}{(\nu-\widetilde{T}+t)^{\mu}}d\nu\\ &=\frac{-1}{\Gamma(1-\mu)}\frac{d}{dt}\int_{0}^{t}\frac{\mathscr{V}(\xi,\widetilde{T}-\tilde{\xi})-\mathscr{V}(\xi,\widetilde{T})}{(t-\tilde{\xi})^{\mu}}d\tilde{\xi}\quad(\text{ using }\ \nu=\widetilde{T}-\tilde{\xi})\\ &=\frac{-1}{\Gamma(1-\mu)}\frac{d}{dt}\int_{0}^{t}\frac{u(x,\tilde{\xi})-u(x,0)}{(t-\tilde{\xi})^{\mu}}d\tilde{\xi}.\end{aligned}$$

Now defining

$$ {}_0D_t^{\mu}u(\varkappa,t) = \frac{1}{\Gamma(1-\mu)}\frac{d}{dt}\int_0^t \frac{u(\varkappa,\tilde{\xi})-u(\varkappa,0)}{(t-\tilde{\xi})^{\mu}}d\tilde{\xi}, \quad (0<\mu<1), $$

we have

$$ \frac{\partial^{\mu}\mathscr{V}(\xi,\tau)}{\partial\tau^{\mu}} = -{}_0D_t^{\mu}u(\varkappa,t). $$

Therefore, letting $\xi = e^{x}$ and denoting $u(\varkappa,t) = \mathscr{V}(e^{x},\widetilde{T}-t)$, we rewrite (3–4) as follows

$$ {}_0D_t^{\mu}u(\varkappa,t) = \frac{\sigma^2}{2}\frac{\partial^2 u(\varkappa,t)}{\partial\varkappa^2} + \left(r_f - \frac{\sigma^2}{2}\right)\frac{\partial u(\varkappa,t)}{\partial\varkappa} - r_f u(\varkappa,t), \quad (\varkappa,t)\in\mathbb{R}\times(0,\widetilde{T}), \tag{6} $$

with

$$ \begin{cases} u(\varkappa,0) = z(\varkappa), \\ u(-\infty,t) = \mathscr{H}(t), \\ u(\infty,t) = \mathscr{G}(t). \end{cases} \tag{7} $$

The modified Riemann–Liouville fractional time derivative operator ${}_0D_t^{\mu}$ can be transformed into the Caputo fractional time derivative operator ${}_0^{C}D_t^{\mu}$ for $0<\mu\le 1$ following (Zhang et al. 2016a):

$$ \begin{aligned} {}_0D_t^{\mu}u(\varkappa,t) &= \frac{1}{\Gamma(1-\mu)}\frac{d}{dt}\int_0^t \frac{u(\varkappa,\tilde{\xi})-u(\varkappa,0)}{(t-\tilde{\xi})^{\mu}}d\tilde{\xi} \\ &= \frac{1}{\Gamma(1-\mu)}\frac{d}{dt}\int_0^t \frac{u(\varkappa,\tilde{\xi})}{(t-\tilde{\xi})^{\mu}}d\tilde{\xi} - \frac{1}{\Gamma(1-\mu)}\frac{d}{dt}\int_0^t \frac{u(\varkappa,0)}{(t-\tilde{\xi})^{\mu}}d\tilde{\xi} \\ &= \frac{1}{\Gamma(1-\mu)}\frac{d}{dt}\int_0^t \frac{u(\varkappa,\tilde{\xi})}{(t-\tilde{\xi})^{\mu}}d\tilde{\xi} - \frac{t^{-\mu}}{\Gamma(1-\mu)}u(\varkappa,0) \\ &= \frac{1}{\Gamma(1-\mu)}\int_0^t (t-\tilde{\xi})^{-\mu}\frac{\partial u(\varkappa,\tilde{\xi})}{\partial\tilde{\xi}}d\tilde{\xi} \\ &= {}_0^{C}D_t^{\mu}u(\varkappa,t). \end{aligned} $$

Lastly, to solve the problem numerically, we need to truncate the unbounded domain into a finite interval (I_p,F_p). Also, without loss of generality we add a source term to the RHS of the Eq. (6). Thus, we have the following problem

$$ {}_0^{C}D_t^{\mu}u(\varkappa,t) = \alpha\frac{\partial^2 u(\varkappa,t)}{\partial\varkappa^2} + \beta\frac{\partial u(\varkappa,t)}{\partial\varkappa} - \gamma u(\varkappa,t) + \psi(\varkappa,t), \quad (\varkappa,t)\in(I_p,F_p)\times(0,\widetilde{T}), \tag{8} $$

with

$$\begin{cases} u(\varkappa,0) = z(\varkappa), \\ u(I_p,t) = \mathscr{H}(t), \\ u(F_p,t) = \mathscr{G}(t), \end{cases} \tag{9}$$

where $\alpha = \frac{\sigma^2}{2} > 0$, $\beta = r_f - \frac{\sigma^2}{2}$, and $\gamma = r_f > 0$. From the above fractional Black–Scholes model, we can obtain the widely known reaction-diffusion model by taking $\alpha > 0$, $\beta = 0$, and $\gamma \neq 0$, and the time fractional advection-diffusion model by taking $\alpha > 0$, $\beta < 0$, and $\gamma = 0$. One find several works for both the models, but from the existing literature, it seems that the work on the time-fractional Black–Scholes model is comparatively less and confined. Therefore, in this paper, we have considered the time-fractional Black–Scholes model to solve it numerically using the collocation method based on the exponential B-spline functions.

3 Numerical Scheme

3.1 Outline of the Exponential B-spline Functions

Consider the uniform partition $\Pi_\varkappa$ of the interval $[I_p, F_p]$, with nodes $\varkappa_m = I_p + mh_\varkappa$ for $m = 0, 1, 2, \ldots, N_\varkappa$. Here, $h_\varkappa = \frac{(F_p - I_p)}{N_\varkappa}$ denotes the mesh spacing in the spatial direction. Suppose

$$\tilde{s} = \sinh(\rho h_\varkappa),$$
$$\tilde{c} = \cosh(\rho h_\varkappa).$$

Here, the tension parameter ρ is restricted to non-negative values.

McCartin (1991) put forth an innovative generalization of the cubic spline, which is now known as the exponential spline. An essential aspect of the exponential spline is the non-negative tension parameter, which facilitates the incorporation of stiffness characteristics in multiple spline segments. In addition to the partition $\Pi_\varkappa$ mentioned above, the definition of exponential B-spline functions encompasses six more points $\varkappa_i$, where $i = -3, -2, -1, N_\varkappa + 1, N_\varkappa + 2, N_\varkappa + 3$. It is worth noting that these additional points are situated outside the interval $[I_p, F_p]$. The following representation outlines the definition of the exponential B-spline functions $\mathscr{Q}_m(\varkappa)$:

$$\mathscr{Q}_m(\varkappa) = \begin{cases} \tilde{r}(\varkappa_{m-2} - \varkappa) - \frac{\tilde{r}}{\rho}\sinh(\rho(\varkappa_{m-2} - \varkappa)), & \varkappa \in [\varkappa_{m-2}, \varkappa_{m-1}], \\ \tilde{a} + \tilde{b}(\varkappa_m - \varkappa) + \bar{c}e^{\rho(\varkappa_m - \varkappa)} + qe^{-\rho(\varkappa_m - \varkappa)}, & \varkappa \in [\varkappa_{m-1}, \varkappa_m], \\ \tilde{a} + \tilde{b}(\varkappa - \varkappa_m) + \bar{c}e^{\rho(\varkappa - \varkappa_m)} + qe^{-\rho(\varkappa - \varkappa_m)}, & \varkappa \in [\varkappa_m, \varkappa_{m+1}], \\ \tilde{r}(\varkappa - \varkappa_{m+2}) - \frac{\tilde{r}}{\rho}\sinh(\rho(\varkappa - \varkappa_{m+2})), & \varkappa \in [\varkappa_{m+1}, \varkappa_{m+2}], \\ 0, & otherwise, \end{cases} \tag{10}$$

where $m = -1, 0, \ldots, N_x, N_x + 1$, and

$$\tilde{r} = \frac{\rho}{2(\rho h_x \tilde{c} - \tilde{s})}, \quad \tilde{a} = \frac{\rho h_x \tilde{c}}{\rho h_x \tilde{c} - \tilde{s}}, \quad \tilde{b} = \frac{\rho}{2}\left[\frac{\tilde{c}(\tilde{c}-1) + \tilde{s}^2}{(\rho h_x \tilde{c} - \tilde{s})(1-\tilde{c})}\right],$$
$$\bar{c} = \frac{1}{4}\left[\frac{e^{-\rho h_x}(1-\tilde{c}) + \tilde{s}(e^{-\rho h_x} - 1)}{(\rho h_x \tilde{c} - \tilde{s})(1-\tilde{c})}\right],$$
$$q = \frac{1}{4}\left[\frac{e^{\rho h_x}(\tilde{c}-1) + \tilde{s}(e^{\rho h_x} - 1)}{(\rho h_x \tilde{c} - \tilde{s})(1-\tilde{c})}\right].$$

Over the entire real line $\mathbb{R}$, the exponential B-spline functions $\mathscr{Q}_{-1}(x)$, $\mathscr{Q}_0(x)$, …, $\mathscr{Q}_{N_x}(x)$, and $\mathscr{Q}_{N_x+1}(x)$ are twice continuously differentiable and exhibit local support. Within the interval $[I_p, F_p]$, the collection $\{\mathscr{Q}_m(x)\}_{m=-1}^{N_x+1}$ is both linearly independent and constitutes a basis for the exponential B-spline space $\mathscr{W}_{N_x+3} = \text{span}\left(\{\mathscr{Q}_m(x)\}_{m=-1}^{N_x+1}\right)$. Table 1 provides the values of $\mathscr{Q}_m(x)$, $\mathscr{Q}'_m(x)$, and $\mathscr{Q}''_m(x)$ at every mesh point.

3.2 A Fully Discrete Numerical Scheme

In this sub-section, first we will discretize the Caputo time-fractional derivative and then derive the fully-discretized numerical scheme. Let the interval $[0, \widetilde{T}]$ is uniformly partitioned by Π_t, defined as $0 = t_0 < t_1 < \cdots < t_{N_t-1} < t_{N_t} = \widetilde{T}$, where $t_n = nh_t$, $n = 0, 1, 2, \cdots, N_t$, with $h_t = \frac{\widetilde{T}}{N_t}$ is the mesh spacing in the time direction. We approximate the Caputo time fractional derivative ${}_0^C D_t^\mu u(x,t)$ at t_{n+1}, $n = -1, 0, \cdots, N_t - 1$, using $L1$ method (Li and Zeng 2019) as follows

$$\begin{aligned}
{}_0^C D_t^\mu u(x, t_{n+1}) &= \frac{1}{\Gamma(1-\mu)} \int_0^{t_{n+1}} (t_{n+1} - s)^{-\mu} \frac{\partial u}{\partial s}(x, s) ds \\
&= \frac{1}{\Gamma(1-\mu)} \sum_{k=0}^{n} \int_{t_k}^{t_{k+1}} (t_{n+1} - s)^{-\mu} \left[\frac{u(x, t_{k+1}) - u(x, t_k)}{h_t}\right] ds + \mathcal{R}^{n+1} \\
&= \frac{h_t^{-\mu}}{\Gamma(2-\mu)} \sum_{k=0}^{n} \omega_k^{(\mu)} \left[u(x, t_{n-k+1}) - u(x, t_{n-k})\right] + \mathcal{R}^{n+1},
\end{aligned} \tag{11}$$

where $\omega_k^{(\mu)} = (k+1)^{1-\mu} - (k)^{1-\mu}$ and the truncation error $\mathcal{R}^{n+1}$ is bounded by

Table 1 The values of $\mathscr{Q}_m(x)$, $\mathscr{Q}'_m(x)$, and $\mathscr{Q}''_m(x)$ at each mesh point

	$\mathscr{Q}_m(x_i)$	$\mathscr{Q}'_m(x_i)$	$\mathscr{Q}''_m(x_i)$
$i = m$	1	0	$\frac{-\rho^2 \tilde{s}}{\rho h_x \tilde{c} - \tilde{s}}$
$i = m \pm 1$	$\frac{\tilde{s} - \rho h_x}{2(\rho h_x \tilde{c} - \tilde{s})}$	$\frac{\mp \rho(\tilde{c}-1)}{2(\rho h_x \tilde{c} - \tilde{s})}$	$\frac{\rho^2 \tilde{s}}{2(\rho h_x \tilde{c} - \tilde{s})}$
Else	0	0	0

$$|\mathcal{R}^{n+1}| \leq k_1 h_t^{2-\mu}, \tag{12}$$

where k_1 is a constant.

Lemma 1 *The coefficients* $\omega_k^{(\mu)}$ *satisfy* (*Singh and Kumar* 2023)

(i) $\omega_0^{(\mu)} = 1$,
(ii) $\omega_k^{(\mu)} > 0, \ \ 0 \leq k \leq n$,
(iii) $< \omega_k^{(\mu)} >$ *is monotonic decreasing sequence*,
(iv) $\sum_{k=0}^{n} \left(\omega_k^{(\mu)} - \omega_{k+1}^{(\mu)}\right) + \omega_{n+1}^{(\mu)} = 1$.

At time level $n+1$, the Eq. (8) takes the form

$$\begin{aligned} {}_0^C D_t^{\mu} u(\varkappa, t_{n+1}) &= \alpha \frac{\partial^2 u^{n+1}(\varkappa)}{\partial \varkappa^2} \\ &+ \beta \frac{\partial u^{n+1}(\varkappa)}{\partial \varkappa} - \gamma u^{n+1}(\varkappa) + \psi^{n+1}(\varkappa). \end{aligned} \tag{13}$$

Now we discretize Eq. (13). Substitution of Eq. (11) in Eq. (13) gives

$$\begin{aligned} &\sum_{k=0}^{n} \omega_k^{(\mu)} \left[u(\varkappa, t_{n-k+1}) - u(\varkappa, t_{n-k})\right] + \mathcal{R}^{n+1} \\ &= \alpha\widetilde{\gamma} \frac{\partial^2 u^{n+1}(\varkappa)}{\partial \varkappa^2} \\ &\quad + \beta\widetilde{\gamma} \frac{\partial u^{n+1}(\varkappa)}{\partial \varkappa} - \gamma\widetilde{\gamma} u^{n+1}(\varkappa) \\ &\quad + \widetilde{\gamma}\psi^{n+1}(\varkappa), \ \ (-1 \leq n \leq N_t - 1), \end{aligned} \tag{14}$$

with

$$\begin{cases} u^0(\varkappa) = z(\varkappa), \\ u^{n+1}(I_p) = \mathscr{H}(t_{n+1}), \ \ -1 \leq n \leq N_t - 1, \\ u^{n+1}(F_p) = \mathscr{G}(t_{n+1}), \ \ -1 \leq n \leq N_t - 1, \end{cases} \tag{15}$$

where

$$\widetilde{\gamma} = \Gamma(2-\mu) h_t^{\mu}.$$

We express the approximate solution $\mathscr{U}^{n+1}(\varkappa)$ to the analytical solution $u^{n+1}(\varkappa)$ of problem (8)–(9) in the following manner:

$$\mathscr{U}^{n+1}(\varkappa) = \sum_{m=-1}^{N_\varkappa+1} \mathscr{R}_m^{n+1}\, \mathscr{Q}_m(\varkappa), \tag{16}$$

where the unknown coefficients $\mathscr{R}_m^{n+1}$, require determination. By employing Table 1, we can obtain expressions for $\mathscr{U}^{n+1}(\varkappa_m)$, $\mathscr{U}_\varkappa^{n+1}(\varkappa_m)$, and $\mathscr{U}_{\varkappa\varkappa}^{n+1}(\varkappa_m)$ at each $-1 \le m \le N_\varkappa + 1$, all in terms of the coefficients $\mathscr{R}_m^{n+1}$

$$\mathscr{U}^{n+1}(\varkappa_m) = \eta\mathscr{R}_{m-1}^{n+1} + \mathscr{R}_m^{n+1} + \eta\mathscr{R}_{m+1}^{n+1}, \tag{17}$$

$$\mathscr{U}_\varkappa^{n+1}(\varkappa_m) = \tilde{e}(\tilde{c}-1)\left[\mathscr{R}_{m+1}^{n+1} - \mathscr{R}_{m-1}^{n+1}\right], \tag{18}$$

$$\mathscr{U}_{\varkappa\varkappa}^{n+1}(\varkappa_m) = \bar{\eta}\left[\mathscr{R}_{m-1}^{n+1} - 2\mathscr{R}_m^{n+1} + \mathscr{R}_{m+1}^{n+1}\right], \tag{19}$$

where

$$\eta = \frac{\tilde{s} - \rho h_\varkappa}{2(\rho h_\varkappa \tilde{c} - \tilde{s})}, \qquad \tilde{e} = \frac{\rho}{2(\rho h_\varkappa \tilde{c} - \tilde{s})}, \qquad \bar{\eta} = \frac{\rho^2 \tilde{s}}{2(\rho h_\varkappa \tilde{c} - \tilde{s})}.$$

Now the discretization of (14) at $\varkappa = \varkappa_m$ gives

$$\begin{aligned}
&\sum_{k=0}^{n} \omega_k^{(\mu)} \left[u(\varkappa_m, t_{n-k+1}) - u(\varkappa_m, t_{n-k})\right] + \mathcal{R}^{n+1} \\
&\quad = \alpha\widetilde{\gamma}\frac{\partial^2 u^{n+1}(\varkappa_m)}{\partial \varkappa_m^2} \\
&\quad + \beta\widetilde{\gamma}\frac{\partial u^{n+1}(\varkappa_m)}{\partial \varkappa_m} - \gamma\widetilde{\gamma}u^{n+1}(\varkappa_m) \\
&\quad + \widetilde{\gamma}\psi^{n+1}(\varkappa_m), \quad (0 \le m \le N_\varkappa, -1 \le n \le N_t - 1).
\end{aligned} \tag{20}$$

The collocation conditions are satisfied by the exponential B-spline function $\mathscr{U}^{n+1}(\varkappa)$, which can be expressed as follows

$$\begin{aligned}
&\sum_{k=0}^{n} \omega_k^{(\mu)} \left[\mathscr{U}^{n-k+1}(\varkappa_m) - \mathscr{U}^{n-k}(\varkappa_m)\right] \\
&\quad = \alpha\widetilde{\gamma}\frac{\partial^2 \mathscr{U}^{n+1}(\varkappa_m)}{\partial \varkappa^2} \\
&\quad + \beta\widetilde{\gamma}\frac{\partial \mathscr{U}^{n+1}(\varkappa_m)}{\partial \varkappa} - \gamma\widetilde{\gamma}\mathscr{U}^{n+1}(\varkappa_m) \\
&\quad + \widetilde{\gamma}\psi^{n+1}(\varkappa_m), \quad (0 \le m \le N_\varkappa, -1 \le n \le N_t - 1),
\end{aligned} \tag{21}$$

$$\begin{cases} \mathscr{U}^{0}(\varkappa_m) = z_m, & 0 \le m \le N_\varkappa, \\ \mathscr{U}^{n+1}(\varkappa_0) = \mathscr{H}_{n+1}, & -1 \le n \le N_t - 1, \\ \mathscr{U}^{n+1}(\varkappa_{N_\varkappa}) = \mathscr{G}_{n+1}, & -1 \le n \le N_t - 1, \end{cases} \tag{22}$$

where $z(\varkappa_m) = z_m$, $\mathscr{H}(t_{n+1}) = \mathscr{H}_{n+1}$, and $\mathscr{G}(t_{n+1}) = \mathscr{G}_{n+1}$.

Now the substitution of the Eqs. (17), (18), and (19) in Eq. (21), and the substitution of Eq. (17) in boundary conditions given in Eq. (22) yield

$$\begin{aligned} &\chi_1 \mathscr{R}_{m-1}^{n+1} + \chi_2 \mathscr{R}_{m}^{n+1} + \chi_3 \mathscr{R}_{m+1}^{n+1} = \eta \mathscr{R}_{m-1}^{n} + \mathscr{R}_{m}^{n} \\ &\quad + \eta \mathscr{R}_{m+1}^{n} - \sum_{k=1}^{n} \omega_k^{(\mu)} [(\eta \mathscr{R}_{m-1}^{n-k+1} + \mathscr{R}_{m}^{n-k+1} + \eta \mathscr{R}_{m+1}^{n-k+1}) \\ &- (\eta \mathscr{R}_{m-1}^{n-k} + \mathscr{R}_{m}^{n-k} + \eta \mathscr{R}_{m+1}^{n-k})] + \widetilde{\gamma} \psi^{n+1}(\varkappa_m), \end{aligned} \tag{23}$$

and

$$\eta \mathscr{R}_{-1}^{n+1} = \mathscr{H}_{n+1} - \mathscr{R}_{0}^{n+1} - \eta \mathscr{R}_{1}^{n+1}, \tag{24}$$

$$\eta \mathscr{R}_{N_\varkappa+1}^{n+1} = \mathscr{G}_{n+1} - \mathscr{R}_{N_\varkappa}^{n+1} - \eta \mathscr{R}_{N_\varkappa-1}^{n+1}, \tag{25}$$

where

$$\begin{aligned} \chi_1 &= \eta - \alpha\gamma\bar{\eta} + \beta\gamma\tilde{e}(\tilde{c} - 1) + \eta\gamma\gamma, \\ \chi_2 &= 1 + 2\alpha\gamma\bar{\eta} + \gamma\gamma, \\ \chi_3 &= \eta - \alpha\gamma\bar{\eta} - \beta\gamma\tilde{e}(\tilde{c} - 1) + \eta\gamma\gamma. \end{aligned}$$

By considering the system (23), we can eliminate the unknown coefficients $\mathscr{R}_{-1}^{n+1}$ and $\mathscr{R}_{N_\varkappa+1}^{n+1}$ through the utilization of Eqs. (24) and (25) respectively. Ultimately, for every time step n, we end up with a tri-diagonal system that involves $(N_\varkappa + 1)$ equations and $(N_\varkappa + 1)$ unknowns, and it can be conveniently solved using the Thomas algorithm. We have

$$S\mathscr{R}^{n+1} = Q\left(\mathscr{R}^{n} - \sum_{k=1}^{n} \omega_k^{(\mu)} (\mathscr{R}^{n-k+1} - \mathscr{R}^{n-k}) \right) + B, \tag{26}$$

where

$$S = \begin{pmatrix} \mathscr{E}_1 & \mathscr{E}_2 & 0 & .. & 0 & 0 & 0 \\ \chi_1 & \chi_2 & \chi_3 & .. & 0 & 0 & 0 \\ 0 & \chi_1 & \chi_2 & .. & 0 & 0 & 0 \\ & & & .. & & & \\ 0 & 0 & 0 & .. & \chi_2 & \chi_3 & 0 \\ 0 & 0 & 0 & .. & \chi_1 & \chi_2 & \chi_3 \\ 0 & 0 & 0 & .. & 0 & -\mathscr{E}_2 & \mathscr{E}_3 \end{pmatrix},$$

$$\mathscr{R}^n = \begin{pmatrix} \mathscr{R}_0^n \\ \mathscr{R}_1^n \\ . \\ . \\ . \\ \mathscr{R}_{M-1}^n \\ \mathscr{R}_M^n \end{pmatrix}, \qquad Q = \begin{pmatrix} 0 & 0 & 0 & ..... & 0 & 0 & 0 \\ \eta & 1 & \eta & ..... & 0 & 0 & 0 \\ 0 & \eta & 1 & ..... & 0 & 0 & 0 \\ & & & ..... & & & \\ 0 & 0 & 0 & ..... & 1 & \eta & 0 \\ 0 & 0 & 0 & ..... & \eta & 1 & \eta \\ 0 & 0 & 0 & ..... & 0 & 0 & 0 \end{pmatrix},$$

$$\mathscr{E}_1 = \alpha\widetilde{\gamma}\bar{\eta}\left(2 + \frac{1}{\eta}\right) - \frac{\beta\widetilde{\gamma}\tilde{e}(\tilde{c}-1)}{\eta},$$

$$\mathscr{E}_2 = -2\beta\widetilde{\gamma}\tilde{e}(\tilde{c}-1),$$

$$\mathscr{E}_3 = \alpha\widetilde{\gamma}\bar{\eta}\left(2 + \frac{1}{\eta}\right) + \frac{\beta\widetilde{\gamma}\tilde{e}(\tilde{c}-1)}{\eta},$$

and

$$B = \begin{pmatrix} \mathscr{H}_n - \sum_{k=1}^{n} \omega_k^{(\mu)}(\mathscr{H}_{n-k+1} - \mathscr{H}_{n-k}) - \frac{\chi_1}{\eta}\mathscr{H}_{n+1} + \widetilde{\gamma}\psi^{n+1}(\varkappa_0) \\ \widetilde{\gamma}\psi^{n+1}(\varkappa_1) \\ \widetilde{\gamma}\psi^{n+1}(\varkappa_2) \\ . \\ . \\ . \\ \widetilde{\gamma}\psi^{n+1}(\varkappa_{N_x-1}) \\ \mathscr{G}_n - \sum_{k=1}^{n} \omega_k^{(\mu)}(\mathscr{G}_{n-k+1} - \mathscr{G}_{n-k}) - \frac{\chi_3}{\eta}\mathscr{G}_{n+1} + \widetilde{\gamma}\psi^{n+1}(\varkappa_{N_x}) \end{pmatrix}.$$

We observe that the set of systems in (26) for $n = 0, 1, \cdots, N_t$, can be solved recursively if we know the initial vector $\mathscr{R}^0$. Note that $\mathscr{R}_{-1}^0$ and $\mathscr{R}_{N_x+1}^0$ can be then calculated using Eqs. (24) and (25) respectively.

3.3 Initial Vector Estimation

In order to initiate the process, it is essential to have an appropriate initial vector $\mathscr{R}^0$ for the system. In this regard, we take into account the initial conditions stated in (22)

$$\mathscr{U}_x^0(I_p) = z'(I_p), \qquad \mathscr{U}_x^0(F_p) = z'(F_p).$$

Now, we proceed to substitute the Eq. (18) into the preceding two equations, leading to:

$$\mathscr{U}_{\varkappa}^{0}(\varkappa_0) = \mathscr{U}_{\varkappa}^{0}(I_p) = \tilde{e}(\tilde{c}-1)[\mathscr{R}_{1}^{0} - \mathscr{R}_{-1}^{0}] = z'(I_p), \tag{27}$$

$$\mathscr{U}_{\varkappa}^{0}(\varkappa_{N_\varkappa}) = \mathscr{U}_{\varkappa}^{0}(F_p) = \tilde{e}(\tilde{c}-1)[\mathscr{R}_{N_\varkappa+1}^{0} - \mathscr{R}_{N_\varkappa-1}^{0}] = z'(F_p). \tag{28}$$

Additionally, incorporating the relation (17) along with the initial condition in (22), results in an algebraic system comprising $(N_\varkappa + 1)$ equations

$$\mathscr{U}^{0}(\varkappa_m) = \eta\mathscr{R}_{m-1}^{0} + \mathscr{R}_{m}^{0} + \eta\mathscr{R}_{m+1}^{0} = z_m, \quad m = 0, 1, \cdots, N_\varkappa, \tag{29}$$

with unknowns $\mathscr{R}_{-1}^{0}, \mathscr{R}_{0}^{0}, \mathscr{R}_{1}^{0}, \ldots, \mathscr{R}_{N_\varkappa-1}^{0}, \mathscr{R}_{N_\varkappa}^{0}, \mathscr{R}_{N_\varkappa+1}^{0}$. The utilization of Eqs. (27) and (28) allows us to eliminate $\mathscr{R}_{-1}^{0}$ and $\mathscr{R}_{N_\varkappa+1}^{0}$. Finally, we end up with a tri-diagonal system that involves $(N_\varkappa + 1)$ equations and $(N_\varkappa + 1)$ unknowns, and it can be conveniently solved using the Thomas algorithm. We have

$$T\mathscr{R}^{0} = \mathscr{C}, \tag{30}$$

where

$$T = \begin{pmatrix} 1 & 2\eta & 0 & ..... & 0 & 0 & 0 \\ \eta & 1 & \eta & ..... & 0 & 0 & 0 \\ 0 & \eta & 1 & ..... & 0 & 0 & 0 \\ & & & ..... & & & \\ 0 & 0 & 0 & ..... & 1 & \eta & 0 \\ 0 & 0 & 0 & ..... & \eta & 1 & \eta \\ 0 & 0 & 0 & ..... & 0 & 2\eta & 1 \end{pmatrix},$$

$$\mathscr{R}^{0} = \begin{pmatrix} \mathscr{R}_{0}^{0} \\ \mathscr{R}_{1}^{0} \\ . \\ . \\ . \\ \mathscr{R}_{N_\varkappa-1}^{0} \\ \mathscr{R}_{N_\varkappa}^{0} \end{pmatrix}, \qquad \mathscr{C} = \begin{pmatrix} z_0 + \frac{\eta}{\tilde{e}(\tilde{c}-1)}z'(I_p) \\ z_1 \\ . \\ . \\ . \\ z_{N_\varkappa-1} \\ z_{N_\varkappa} - \frac{\eta}{\tilde{e}(\tilde{c}-1)}z'(F_p) \end{pmatrix}.$$

4 Stability Analysis

In this section we discuss the stability analysis of the proposed scheme.

Theorem 1 *The numerical scheme* (23) *solving the TFBSM* (8)–(9) *is unconditionally stable*.

Proof Let $\bar{\mathscr{R}}$ be a perturbed solution of the system (23). We will investigate how the perturbation $\delta_m^n = \mathscr{R}_m^n - \bar{\mathscr{R}}_m^n$ develops over time. Note that δ_m^n solves the following equation

$$\begin{aligned}\chi_1\delta_{m-1}^{n+1} + \chi_2\delta_m^{n+1} + \chi_3\delta_{m+1}^{n+1} &= \eta\delta_{m-1}^n \\ &+ \delta_m^n + \eta\delta_{m+1}^n - \sum_{k=1}^{n}\omega_k^{(\mu)}\big[(\eta\delta_{m-1}^{n-k+1} + \delta_m^{n-k+1} + \eta\delta_{m+1}^{n-k+1}) \\ &- (\eta\delta_{m-1}^{n-k} + \delta_m^{n-k} + \eta\delta_{m+1}^{n-k})\big].\end{aligned} \tag{31}$$

Now, to use the von Neumann stability analysis we assume that

$$\delta_m^n = \zeta^n e^{i\varsigma m h_\varkappa}, \tag{32}$$

where $i = \sqrt{-1}$ and ς is the wave number. Inserting the Eq. (32) in (31) yields

$$\zeta^{n+1} = \frac{\Upsilon_1}{(\Upsilon_1 + \Upsilon_2 + \Upsilon_3 - i\Upsilon_4)}\left[\zeta^n - \sum_{k=1}^{n}\omega_k^{(\mu)}(\zeta^{n-k+1} - \zeta^{n-k})\right], \tag{33}$$

where

$$\begin{aligned}&\Upsilon_1 = 1 + 2\eta\cos\varsigma h_\varkappa, \qquad \Upsilon_2 = 2\alpha\widetilde{\gamma}\bar{\eta}(1 - \cos\varsigma h_\varkappa),\\ &\Upsilon_3 = \gamma\widetilde{\gamma}(1 + 2\eta\cos\varsigma h_\varkappa), \quad \text{and} \quad \Upsilon_4 = 2\beta\widetilde{\gamma}\tilde{e}(\tilde{c} - 1)\sin\varsigma h_\varkappa.\end{aligned}$$

From Eq. (33), we have

$$|\zeta^{n+1}|^2 \le \frac{|\Upsilon_1|^2}{\big((\Upsilon_1 + \Upsilon_2 + \Upsilon_3)^2 + \Upsilon_4^2\big)}\left|\left[\zeta^n - \sum_{k=1}^{n}\omega_k^{(\mu)}(\zeta^{n-k+1} - \zeta^{n-k})\right]\right|^2. \tag{34}$$

Since $|\Upsilon_1|^2 < (\Upsilon_1 + \Upsilon_2 + \Upsilon_3)^2 + \Upsilon_4^2$, the Eq. (34) takes the form

$$|\zeta^{n+1}| \le \left|\left[\zeta^n - \sum_{k=1}^{n}\omega_k^{(\mu)}(\zeta^{n-k+1} - \zeta^{n-k})\right]\right|. \tag{35}$$

To show $|\zeta^{n+1}| \le |\zeta^0|$, the mathematical induction is used. For $n = 0$ in Eq. (35) we have $|\zeta^1| \le |\zeta^0|$. Further, we assume that

$$|\zeta^j| \le |\zeta^0|, \qquad j = 1, 2, \ldots, n. \tag{36}$$

Now from the Eq. (35) and using the assumptions in (36) and Lemma 1 we have

$$|\zeta^{n+1}| \le \left|\left[\omega_n^{(\mu)}\zeta^0 + \sum_{k=0}^{n-1}\left(\omega_k^{(\mu)} - \omega_{k+1}^{(\mu)}\right)\zeta^{n-k}\right]\right| \le \left[\omega_n^{(\mu)} + \sum_{k=0}^{n-1}\left(\omega_k^{(\mu)} - \omega_{k+1}^{(\mu)}\right)\right]|\zeta^0| = |\zeta^0|.$$

Hence, the inequality (36) holds for all n. Thus, we observe that the perturbation is bounded at each time level and therefore the numerical scheme (23) solving the TFBSM (8)-(9) is unconditionally stable. This completes the proof. □

5 Convergence Analysis

We now discuss the convergence analysis of the numerical scheme (23). We shall use the following results.

Lemma 2 *Rao and Kumar (2008)For the exponential B-spline space $\mathscr{W}_{N_x+3}$, the basis elements $\{\mathscr{Q}_m(x)\}_{m=-1}^{N_x+1}$ are subject to the following inequality.*

$$\sum_{m=-1}^{N_x+1} |\mathscr{Q}_m(x)| \leq \frac{5}{2}, \qquad I_p \leq x \leq F_p.$$

Theorem 2 *Pruess (1976) Let $\widetilde{V}^{n+1}(x) \in \mathscr{W}_{N_x+3}$, be the unique exponential B-spline interpolant to the exact solution $u^{n+1}(x)$ of problem (8)–(9). If $u \in C^{4,0}[0,1]$ and $\psi \in C^{2,0}[0,1]$, then there exists positive constants c_l such that*

$$\left|\left|\frac{\partial^l}{\partial x^l}\left(u^{n+1}(x) - \widetilde{V}^{n+1}(x)\right)\right|\right|_\infty \leq c_l h_x^{4-l}, \qquad l = 0, 1, 2.$$

Theorem 3 *The collocation approximation $\mathscr{U}^{n+1}(x)$ given in (16) derived from the exponential B-spline space $\mathscr{W}_{N_x+3}$ to the exact solution $u^{n+1}(x)$ of the TFBSM (8)–(9) with $u \in C^{4,0}[0,1]$ and $\psi \in C^{2,0}[0,1]$, satisfies*

$$||u^{n+1}(x) - \mathscr{U}^{n+1}(x)||_\infty \leq \lambda^* h_x^2, \qquad \forall\, n \geq 0,$$

where λ^* is a positive constant independent of h_x.

Proof Consider $\widetilde{V}^{n+1}(x)$ as the unique exponential B-spline interpolant, which uniquely approximates the exact solution $u^{n+1}(x)$ for problem (8)–(9).

$$\widetilde{V}^{n+1}(x) = \sum_{m=-1}^{N_x+1} \mathscr{B}_m^{n+1} \mathscr{Q}_m(x). \tag{37}$$

At time level $n+1$, we can write

$$\begin{aligned} {}_0^C D_t^\mu \widetilde{V}^{n+1}(x) &= \alpha \frac{\partial^2 \widetilde{V}^{n+1}(x)}{\partial x^2} \\ &+ \beta \frac{\partial \widetilde{V}^{n+1}(x)}{\partial x} - \gamma \widetilde{V}^{n+1}(x) + \widetilde{\psi}^{n+1}(x), \quad (-1 \leq n \leq N_t - 1), \end{aligned} \tag{38}$$

with

$$\begin{cases} \widetilde{V}^0(x) = z(x), \\ \widetilde{V}^{n+1}(x_0) = \mathscr{H}(t_{n+1}), \quad -1 \le n \le N_t - 1, \\ \widetilde{V}^{n+1}(x_{N_x}) = \mathscr{G}(t_{n+1}), \quad -1 \le n \le N_t - 1. \end{cases} \tag{39}$$

Now using the Eq. (37) in (38) we have

$$\begin{aligned} &\chi_1 \mathscr{B}_{m-1}^{n+1} + \chi_2 \mathscr{R}_B^{n+1} + \chi_3 \mathscr{B}_{m+1}^{n+1} = \eta \mathscr{B}_{m-1}^{n} \\ &\quad + \mathscr{B}_m^n + \eta \mathscr{B}_{m+1}^n - \sum_{k=1}^{n} \omega_k^{(\mu)} [(\eta \mathscr{B}_{m-1}^{n-k+1} + \mathscr{B}_m^{n-k+1} + \eta \mathscr{B}_{m+1}^{n-k+1}) \\ &\quad - (\eta \mathscr{B}_{m-1}^{n-k} + \mathscr{B}_m^{n-k} + \eta \mathscr{B}_{m+1}^{n-k})] + \widetilde{\gamma} \widetilde{\psi}^{n+1}(x_m), \quad (0 \le m \le N_x, -1 \le n \le N_t - 1), \end{aligned} \tag{40}$$

and also the boundary conditions in (39) together with (37) yield

$$\eta \mathscr{B}_{-1}^{n+1} = \mathscr{H}_{n+1} - \mathscr{B}_0^{n+1} - \eta \mathscr{B}_1^{n+1}, \tag{41}$$

$$\eta \mathscr{B}_{N_x+1}^{n+1} = \mathscr{G}_{n+1} - \mathscr{B}_{N_x}^{n+1} - \eta \mathscr{B}_{N_x-1}^{n+1}. \tag{42}$$

Next, the subtraction of Eq. (23) from (40) gives

$$\begin{aligned} &\chi_1 \lambda_{m-1}^{n+1} + \chi_2 \lambda_m^{n+1} + \chi_3 \lambda_{m+1}^{n+1} = \eta \lambda_{m-1}^{n} + \lambda_m^n \\ &\quad + \eta \lambda_{m+1}^n - \sum_{k=1}^{n} \omega_k^{(\mu)} [(\eta \lambda_{m-1}^{n-k+1} + \lambda_m^{n-k+1} + \eta \lambda_{m+1}^{n-k+1}) \\ &\quad - (\eta \lambda_{m-1}^{n-k} + \lambda_m^{n-k} + \eta \lambda_{m+1}^{n-k})] + \widetilde{\gamma} (\widetilde{\psi}_m^{n+1} - \psi_m^{n+1}), \quad (0 \le m \le N_x, -1 \le n \le N_t - 1). \end{aligned} \tag{43}$$

Also, subtracting Eqs. (24) and (25) from (41) and (42) respectively yield

$$\eta \lambda_{-1}^{n+1} = -\lambda_0^{n+1} - \eta \lambda_1^{n+1}, \qquad -1 \le n \le N_t - 1, \tag{44}$$

$$\eta \lambda_{N_x+1}^{n+1} = -\lambda_{N_x}^{n+1} - \eta \lambda_{N_x-1}^{n+1}, \qquad -1 \le n \le N_t - 1, \tag{45}$$

where $\lambda_m^{n+1} = \mathscr{B}_m^{n+1} - \mathscr{R}_m^{n+1}$ for $-1 \le m \le N_x + 1$ and $-1 \le n \le N_t - 1$.

Now subtracting Eq. (13) from Eq. (38) and using Theorem 2 we have

$$\widetilde{\psi}_m^{n+1} - \psi_m^{n+1} = O(h_x^2).$$

Thus, it follows from the above equation that

$$|\widetilde{\psi}_m^{n+1} - \psi_m^{n+1}| \le M h_x^2, \tag{46}$$

where $M = \frac{c_0 h_x^2 \widetilde{T}}{\Gamma(2-\mu)} + \alpha c_2 + \beta c_1 h_x + \gamma c_0 h_x^2$.

Now, let us take $\widetilde{\lambda}^{n+1} = \max_{-1\le m\le N_x+1} |\lambda_m^{n+1}|$. Also, the initial condition of the problem implies that $\widetilde{\lambda}^0 = 0$. At the first time level, i.e. for $n = 0$, the Eq. (43) can be written as

$$\chi_2\lambda_m^1 = -\chi_1\lambda_{m-1}^1 - \chi_3\lambda_{m+1}^1 + \eta\lambda_{m-1}^0 + \lambda_m^0 + \eta\lambda_{m+1}^0 + \widetilde{\gamma}(\widetilde{\psi}_m^1 - \psi_m^1), \quad 0 \le m \le N_x. \tag{47}$$

By using Taylor's series expansion, for sufficiently small h_x, we have

$$\chi_2\lambda_m^1 = \lambda_m^1(-\chi_1 - \chi_3) + \widetilde{\gamma}(\widetilde{\psi}_m^1 - \psi_m^1). \tag{48}$$

After rearranging the terms and taking the absolute values on both sides of Eq. (48) we have

$$|\lambda_m^1| = \left|\frac{\widetilde{\gamma}(\widetilde{\psi}_m^1 - \psi_m^1)}{(\chi_1 + \chi_2 + \chi_3)}\right| \le \frac{\widetilde{\gamma}Mh_x^2}{(2\eta+1)(1+\gamma\widetilde{\gamma})} \le \widetilde{M}h_x^2, \qquad 0 \le m \le N_x, \tag{49}$$

where $\widetilde{M} = \frac{M\widetilde{\gamma}}{(1+2\eta)(1+\gamma\widetilde{\gamma})}$. Also, from the boundary conditions we have the following estimates for λ_{-1}^1 and $\lambda_{N_x+1}^1$:

$$|\lambda_{-1}^1| \le \widetilde{k}h_x^2 \qquad \text{and} \qquad |\lambda_{N_x+1}^1| \le \widetilde{k}h_x^2, \tag{50}$$

where $\widetilde{k}$ is a constant independent of h_x.

Now combining the inequalities (49) and (50), we have

$$\widetilde{\lambda}^1 \le M_1h_x^2, \tag{51}$$

where $M_1 = \max\{\widetilde{M}, \widetilde{k}\}$.

Next, we use the mathematical induction to prove that $\widetilde{\lambda}^{n+1} \le r^*h_x^2$, where r^* is a positive constant independent of h_x. Therefore, for this purpose we assume that

$$\widetilde{\lambda}^j \le K_jh_x^2 \tag{52}$$

is true for $1 \le j \le n$. Since in Eq. (51) we have shown that result (52) is true for $j = 1$. Now we will prove the result for $j = n + 1$. So, let $\widetilde{K} = \max_{0\le j\le n} K_j$ and write the Eq. (43) in the form

$$\begin{aligned}\chi_2\lambda_m^{n+1} &= -\chi_1\lambda_{m-1}^{n+1}\\ &\quad - \chi_3\lambda_{m+1}^{n+1} + \omega_n^{(\mu)}(\eta\lambda_{m-1}^0 + \lambda_m^0 + \eta\lambda_{m+1}^0)\\ &\quad + \sum_{k=0}^{n-1}\left(\omega_k^{(\mu)} - \omega_{k+1}^{(\mu)}\right)(\eta\lambda_{m-1}^{n-k}\\ &\quad + \lambda_m^{n-k} + \eta\lambda_{m+1}^{n-k}) + \widetilde{\gamma}(\widetilde{\psi}_m^{n+1} - \psi_m^{n+1}), \quad (0 \le m \le N_x).\end{aligned} \tag{53}$$

By applying Taylor's series expansion, for sufficiently small h_x we can have

$$\chi_2\lambda_m^{n+1} = (-\chi_1 - \chi_3)\lambda_m^{n+1} + \omega_n^{(\mu)}(2\eta+1)\lambda_m^0 + (2\eta+1)\sum_{k=0}^{n-1}\left(\omega_k^{(\mu)} - \omega_{k+1}^{(\mu)}\right)\lambda_m^{n-k} + \widetilde{\gamma}(\widetilde{\psi}_m^{n+1} - \psi_m^{n+1}).$$

After rearranging the terms and taking the absolute values on both sides of above equation and using the assumption (52) we have

$$\begin{aligned}(\chi_1+\chi_2+\chi_3)|\lambda_m^{n+1}| \leq & \omega_n^{(\mu)}(2\eta+1)|\lambda_m^0| + (2\eta+1)\sum_{k=0}^{n-1}\left(\omega_k^{(\mu)} - \omega_{k+1}^{(\mu)}\right)|\lambda_m^{n-k}| \\ & + \widetilde{\gamma}|(\widetilde{\psi}_m^{n+1} - \psi_m^{n+1})| \\ \leq & \widetilde{K}(2\eta+1)\left(\sum_{k=0}^{n-1}\left\{\left(\omega_k^{(\mu)} - \omega_{k+1}^{(\mu)}\right) + \omega_n^{(\mu)}\right\}\right)h_x^2 + \widetilde{\gamma}|(\widetilde{\psi}_m^{n+1} - \psi_m^{n+1})|.\end{aligned}$$

$$\text{Thus}, \quad |\lambda_m^{n+1}| \leq \frac{\omega_0^{(\mu)}\widetilde{K}(2\eta+1)h_x^2}{(\chi_1+\chi_2+\chi_3)} + \frac{\widetilde{\gamma}|(\widetilde{\psi}_m^{n+1} - \psi_m^{n+1})|}{(\chi_1+\chi_2+\chi_3)}.$$

Now using the inequality (46) we have

$$|\lambda_m^{n+1}| \leq \frac{\widetilde{K}h_x^2}{(1+\gamma\widetilde{\gamma})} + \frac{\widetilde{\gamma}Mh_x^2}{(2\eta+1)(1+\gamma\widetilde{\gamma})} \leq M^*h_x^2, \qquad 0 \leq m \leq N_x, \tag{54}$$

where $M^* = \frac{\widetilde{K}}{(1+\gamma\widetilde{\gamma})} + \frac{M\widetilde{\gamma}}{(2\eta+1)(1+\gamma\widetilde{\gamma})}$.

Like before as in (50), we can obtain bounds for $|\lambda_{-1}^{n+1}|$ and $|\lambda_{N_x+1}^{n+1}|$. With the help of these two bounds along with (54), it can be inferred that there exists a constant r^* independent of h_x such that

$$\widetilde{\lambda}^{n+1} \leq r^*h_x^2, \tag{55}$$

where $r^* = \max\{M^*, \widetilde{k}\}$.

Now

$$\widetilde{V}^{n+1}(x) - \mathscr{U}^{n+1}(x) = \sum_{m=-1}^{N_x+1}(\mathscr{B}_m^{n+1} - \mathscr{K}_m^{n+1})\mathscr{Q}_m(x).$$

By applying Lemma 2 and utilizing inequality (55), we arrive at

$$||\widetilde{V}^{n+1}(x) - \mathscr{U}^{n+1}(x)||_\infty \leq \frac{5}{2}r^*h_x^2. \tag{56}$$

Using the triangle inequality we get

$$||u^{n+1}(x) - \mathscr{U}^{n+1}(x)||_\infty \leq ||u^{n+1}(x) - \widetilde{V}^{n+1}(x)||_\infty + ||\widetilde{V}^{n+1}(x) - \mathscr{U}^{n+1}(x)||_\infty. \tag{57}$$

Thus, using Theorem 2 and inequality (56), we get

$$||u^{n+1}(x) - \mathscr{U}^{n+1}(x)||_\infty \leq \lambda^* h_x^2, \qquad \forall n \geq 0,$$

where $\lambda^* = \frac{5}{2} r^* + c_0 h_x^2$.

Hence, the proof is complete. □

Theorem 4 *The present numerical scheme* (23) *for the TFBSM* (8)–(9) *is convergent of order* $O(h_t^{2-\mu} + h_x^2)$.

Proof Theorem 3 together with relation (12) provides us the following result

$$||u(x,t) - \mathscr{U}^{n+1}(x)||_\infty \leq k_2 h_t^{2-\mu} + k_3 h_x^2,$$

where k_2 and k_3 are positive constants, and thus the proposed method is convergent of order $O(h_t^{2-\mu} + h_x^2)$. □

6 Numerical Illustrations and Applications

Within this section, we present the numerical outcomes obtained for a test problem involving various options, such as the European call option, European put option, and European double barrier knock-out call option. Furthermore, the advantages of the time-fractional Black–Scholes partial differential equation (PDE) are also outlined in this section. Additionally, as part of the validation process for the proposed numerical scheme, we include the numerical outcomes of three distinct test problems. Notably, one of these problems, namely Example 4, aligns with the classical Black–Scholes PDE. All numerical outcomes from these experiments are available in the Appendix A. Moreover, if $u(x_m, t_n)$ denotes the exact solution and $\mathscr{U}_m^n$ represents the approximate solution of problem (8)–(9) at the point (x_m, t_n), then the accuracy of the numerical solution will be measured as follows

$$L_\infty(h_x, h_t) = ||u(x_m, t_n) - \mathscr{U}_m^n||_\infty = \max_{1\leq n\leq N_t} \max_{1\leq m\leq N_x-1} |u(x_m, t_n) - \mathscr{U}_m^n|, \tag{58}$$

$$L_2(h_x, h_t) = ||u(x_m, t_n) - \mathscr{U}_m^n||_2 = \max_{1\leq n\leq N_t} \sqrt{h_x \sum_{m=1}^{N_x-1} (u(x_m, t_n) - \mathscr{U}_m^n)^2}. \tag{59}$$

By utilizing the following formula, we can evaluate the order of convergence (EOC)

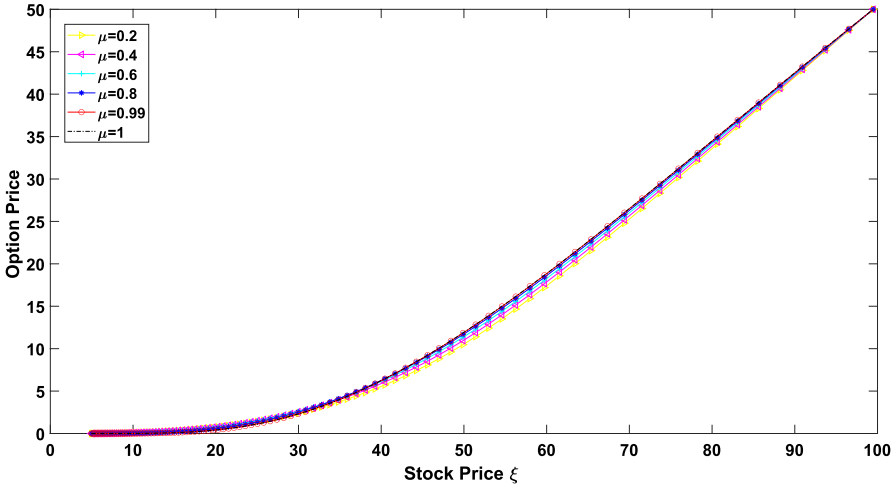

Fig. 1 European call option curves with $\rho = 1.5$, $N_x = N_t = 100$ and different μ for Example 1

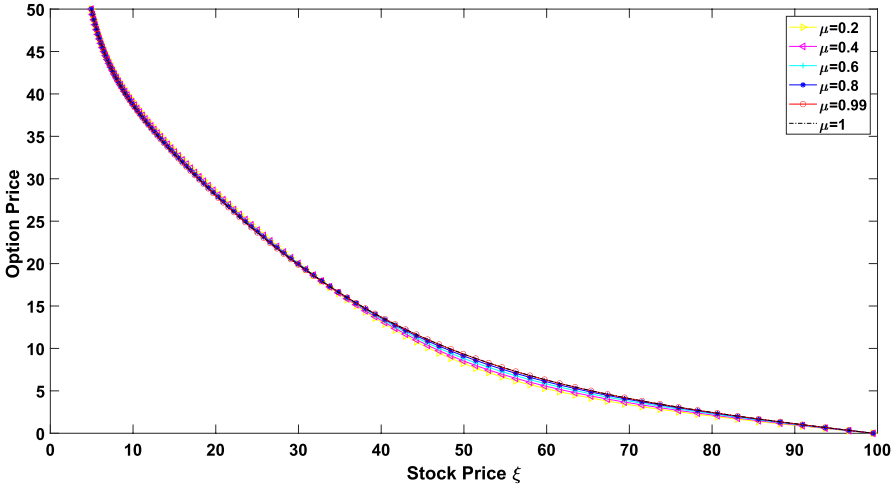

Fig. 2 European put option curves with $\rho = 1.5$, $N_x = N_t = 100$ and different μ for Example 1

$$EOC = \begin{cases} \log_2 \left(\dfrac{L_j(h_x,(h_t)_1)}{L_j(h_x,(h_t)_2)} \right), & \text{in time,} \\ \log_2 \left(\dfrac{L_j((h_x)_1,h_t)}{L_j((h_x)_2,h_t)} \right), & \text{in space,} \end{cases} \tag{60}$$

where $j = 2$ or ∞.

Example 1 Zhang et al. (2016b) Let us consider the TFBSM

$$\begin{aligned}&\frac{\partial^{\mu}\mathcal{V}(\xi,\tau)}{\partial\tau^{\mu}}+\frac{\sigma^2\xi^2}{2}\frac{\partial^2\mathcal{V}(\xi,\tau)}{\partial\xi^2}+(r_f-D_Y)\xi\frac{\partial\mathcal{V}(\xi,\tau)}{\partial\xi}-r_f\mathcal{V}(\xi,\tau)=0,\\&(\xi,\tau)\in(\xi_{I_p},\xi_{F_p})\times(0,\widetilde{T}),\end{aligned}\tag{61}$$

$$\begin{cases}\mathcal{V}(\xi,\widetilde{T})=\phi(\xi),\\ \mathcal{V}(\xi_{I_p},\tau)=\mathscr{H}(\tau),\\ \mathcal{V}(\xi_{F_p},\tau)=\mathscr{G}(\tau).\end{cases}$$

The above model describes different option values depending on the functions $\phi(\xi)$, $\mathscr{H}(\tau)$, and $\mathscr{G}(\tau)$.

- If $\phi(\xi)=\max\{\widetilde{K}-\xi,0\}$, $\mathscr{H}(\tau)=\widetilde{K}e^{-r_f(\widetilde{T}-\tau)}$ and $\mathscr{G}(\tau)=D_Y=0$, then the model represents the European put option.
- If $\phi(\xi)=\max\{\xi-\widetilde{K},0\}$, $\mathscr{H}(\tau)=D_Y=0$ and $\mathscr{G}(\tau)=\xi_{I_f}-\widetilde{K}e^{-r_f(\widetilde{T}-\tau)}$, then the model represents the European call option.
- And if $\phi(\xi)=\max\{\xi-\widetilde{K},0\}$ and $\mathscr{H}(\tau)=\mathscr{G}(\tau)=0$, then the model describes the European double barrier knock-out call option.

For solving European call and European put option models numerically we have taken the parameters $\sigma=0.55$, $r_f=0.05$, $\xi_{I_p}=5(I_p=1.6)$, $\xi_{F_p}=100(F_p=4.6)$, $\widetilde{T}=1$(year), and the strike price $\widetilde{K}=50$. Also, we take the parameters $\sigma=0.55$, $r_f=0.03$, $\xi_{I_p}=3(I_p=1.1)$, $\xi_{F_p}=15(F_p=2.7)$, $\widetilde{T}=1$(year), the dividend yield

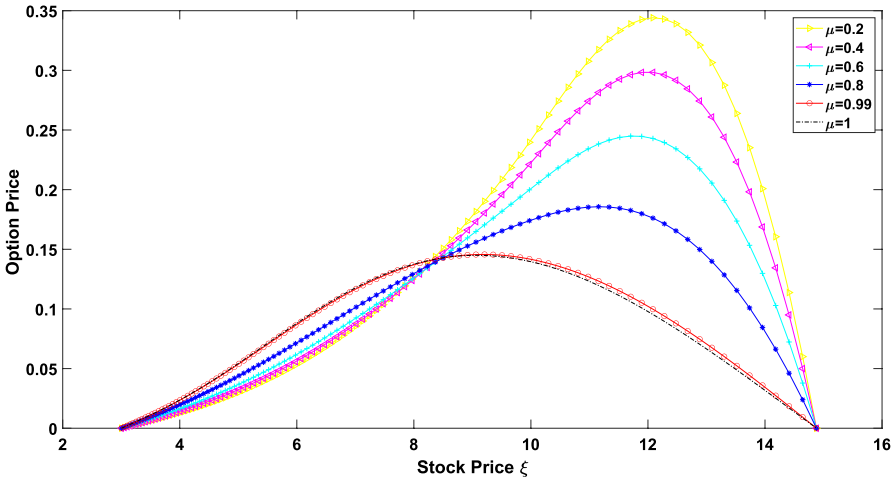

Fig. 3 Double barrier option curves with $\rho=1.5$, $N_x=N_t=150$ and different μ for Example 1

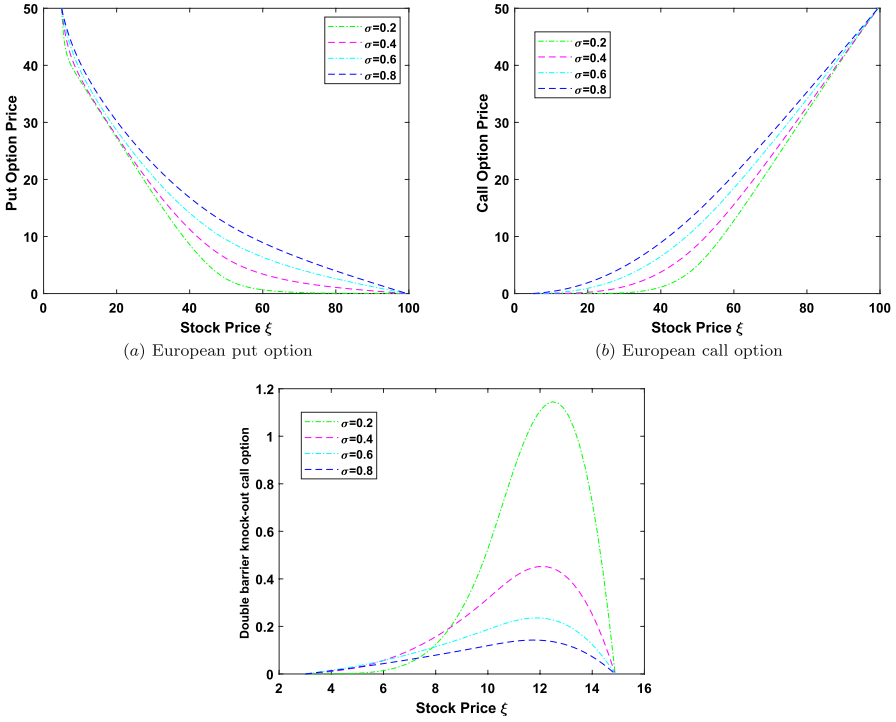

(*a*) European put option

(*b*) European call option

(*c*) European double barrier knock-out call option

Fig. 4 Different option price with $\mu = 0.5$ for multiple σ values

$D_Y = 0.01$, and the strike price $\widetilde{K} = 10$, to study the European double barrier knock-out call option model numerically.

Figures 1 and 2 show how the orders of fractional derivative affect the European call option and put option, respectively. From these two figures, we can observe that when the stock price ξ is less or greater than the strike price $\widetilde{K}$, the option price is slightly affected by the order of the time-fractional derivative. And when the stock price ξ is close to the strike price $\widetilde{K}$, the option price is significantly affected by the time-fractional derivative order. In addition, in Fig. 3, the graph is plotted between the stock price ξ and the double barrier option price $\mathscr{V}$ for various values of time-fractional order μ. It is worth noting here that for $\mu = 1$, the TFBSM converts to the classical Black–Scholes model. Figure 3 depicts that the double barrier option price is highly influenced by the time-fractional order. More specifically, the option price is inversely proportional to the fractional-order when the stock price is greater than or near the strike price $\widetilde{K}$. And the peak of the option price curve occurred corresponding to $\mu = 0.2$. This tells us that TFBSM can explain the jump movement of the problem much more clearly than the classic Black–Scholes model. Further, Fig. 4 illustrates the plotted option prices under various volatility values (σ) for $\mu = 0.5$. These plots reflect, how the stock price volatility influences the option price

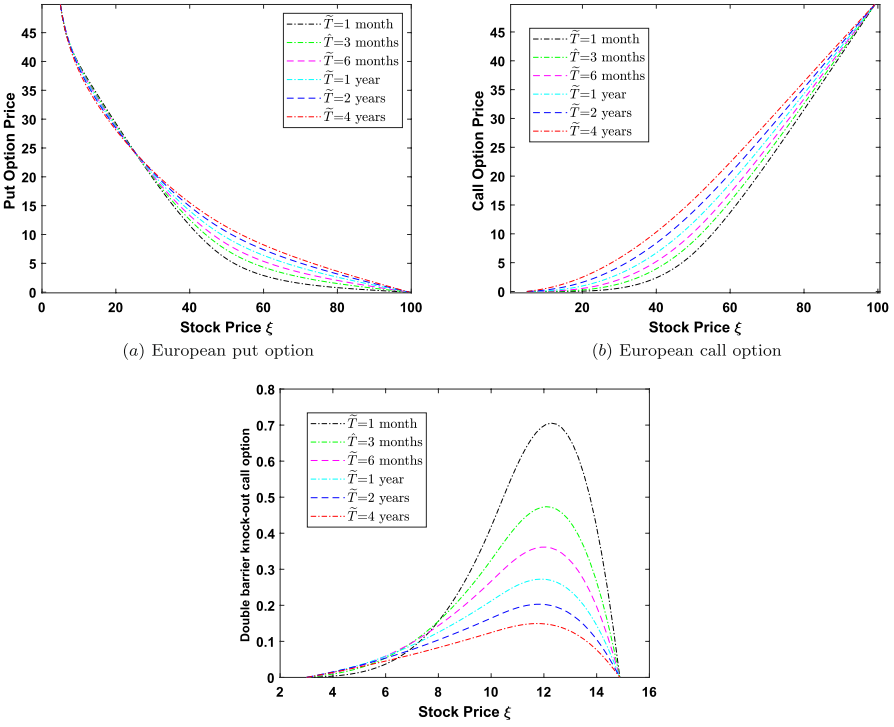

(*a*) European put option (*b*) European call option

(*c*) European double barrier knock-out call opti

Fig. 5 Different option prices with $\mu = 0.5$ at various expiry times $\widetilde{T}$

and supports a well-known statement "The higher the risk, the higher the return". Moreover, In Fig. 5, the option prices at different expiry time ($\widetilde{T}$) for $\mu = 0.5$ are plotted. From this figure, it is evident that when the stock price significantly lags behind the strike price, put opting for a shorter expiration date yields greater profitability compared to choosing a longer expiration date. Conversely, when the stock price is higher, put option with a longer expiration date becomes the more advantageous choice. Whereas, regardless of whether the stock price is lower or higher than the strike price, a call option proves to be consistently advantageous for longer expiry times. In addition to the previous observations, this figure also reveals that the double barrier knock-out call option behaves in direct contrast to the put option. Specifically, when the stock price is higher than the strike price, the double barrier knock-out call option becomes more profitable for shorter expiry times. Along this line, we can observe the behavior of the option prices for varying dividend yields (D_Y) in Fig. 6. By analyzing Fig. 7, a clear inverse relationship between the rate of interest (r_f) and put options becomes evident. In essence, as the rate of interest rises, the value of put options decreases. Conversely, the behavior of call options is contrary to that of put options. Furthermore, our observations indicate that when the stock price significantly falls behind the strike price, opting for a double barrier

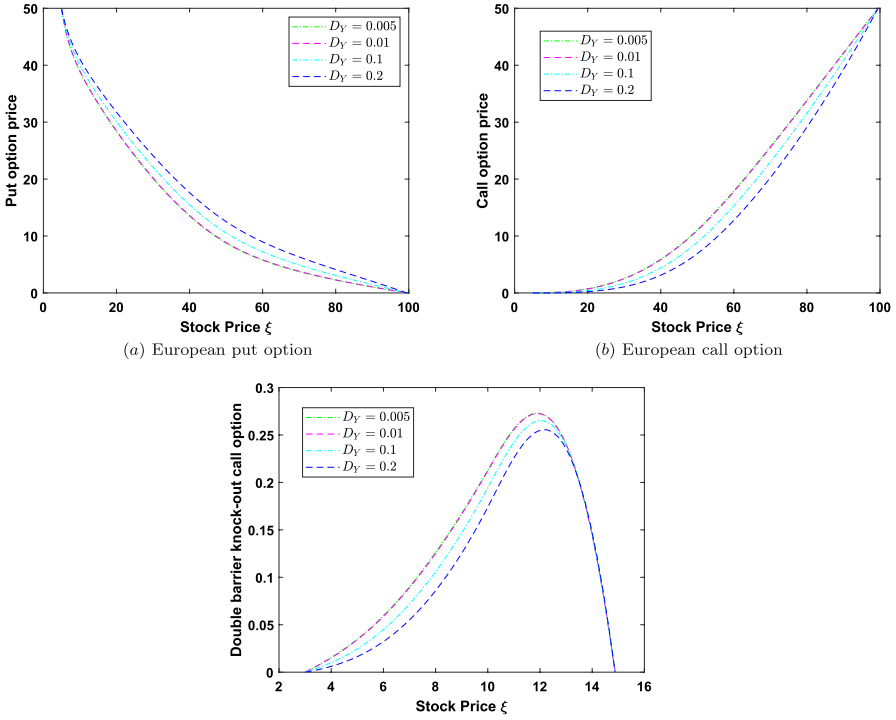

(*a*) European put option

(*b*) European call option

(*c*) European double barrier knock-out call optio

Fig. 6 Different option prices with $\mu = 0.5$ for different dividend yields D_Y

knock-out call option proves more profitable under high-interest rates compared to lower interest rates. However, in situations where the stock price is higher, selecting a double barrier knock-out call option with a lower interest rate emerges as the more advantageous decision. In Fig. 8, the interaction between the option price and strike price ($\widetilde{K}$) is evident. Notably, the put option shows a direct relationship, where an increase in the strike price corresponds to an increase in the option price. In contrast, the call and double barrier knock-out call options manifest an opposite relationship, leading to a decrease in their option prices as the strike price increases.

6.1 Advantages of Time-Fractional Black–Scholes Partial Differential Equation (PDE)

The Black–Scholes partial differential equation is a fundamental equation in financial mathematics used to model the pricing of options. The time-fractional Black–Scholes PDE defined in (3)–(4) is a generalized version of the Black–Scholes PDE that incorporates fractional derivatives with respect to time.

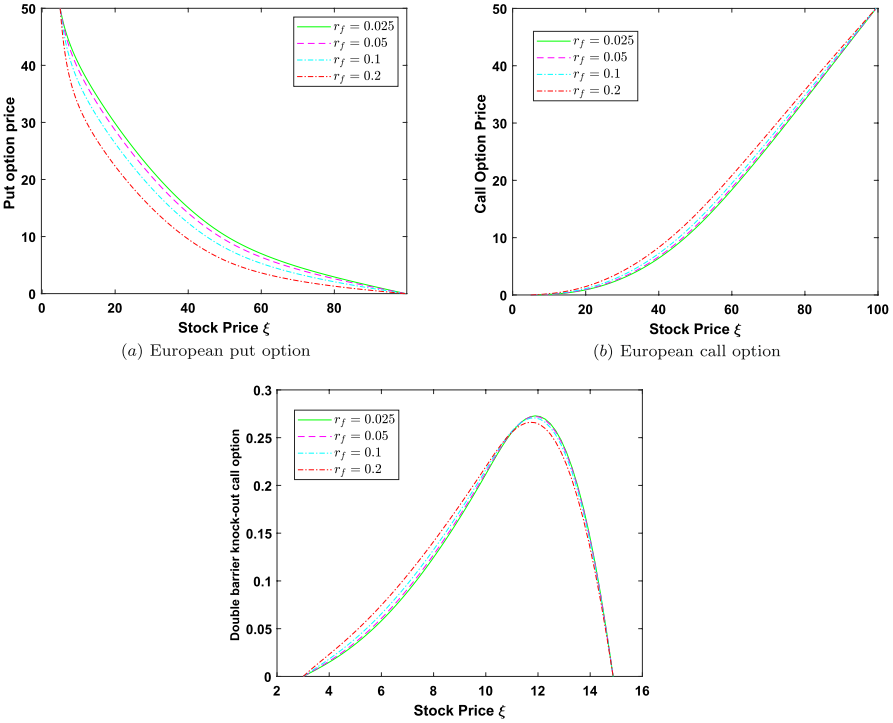

(*a*) European put option

(*b*) European call option

(*c*) European double barrier knock-out call option

Fig. 7 Different option prices with $\mu = 0.5$ for multiple r_f values

This modification allows for more flexibility in modeling complex financial phenomena. Here are a few advantages of the time-fractional Black–Scholes PDE:

(1) *Modeling Market Anomalies* The fractional derivative in the time-fractional Black–Scholes PDE introduces memory effects into the option pricing model. This allows for capturing long-term dependencies and market anomalies that are not adequately captured by the traditional Black–Scholes framework. The time-fractional Black–Scholes PDE can be used to model and price options in markets where memory effects play a significant role, such as markets with persistent volatility or non-Markovian dynamics.

(2) *Option Pricing with Stochastic Volatility* The original Black–Scholes model assumes constant volatility, which is often not realistic. The time-fractional Black–Scholes PDE can incorporate stochastic volatility models by introducing fractional derivatives in both time and volatility. This allows for more accurate pricing of options in markets with time-varying and stochastic volatility, such as in the Heston model or other volatility models.

(3) *Pricing of Exotic Options* Exotic options are derivatives with non-standard features, such as barrier options, Asian options, or lookback options. These options

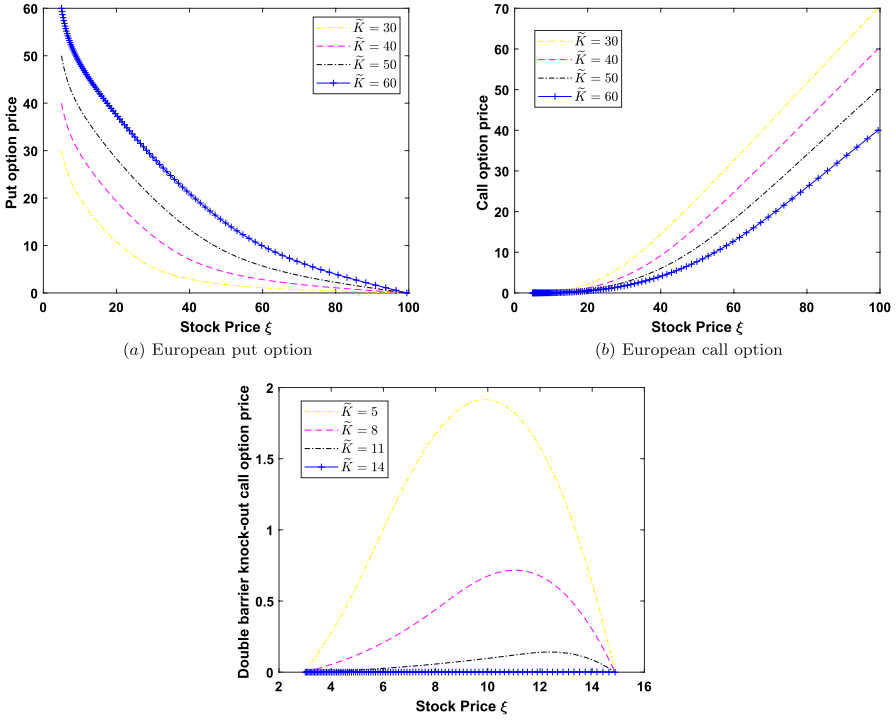

(*a*) European put option

(*b*) European call option

(*c*) European double barrier knock-out call option

Fig. 8 Different option prices with $\mu = 0.5$ for multiple strike prices $\widetilde{K}$ values

often exhibit complex behavior and cannot be easily priced using standard option pricing models. The time-fractional Black–Scholes PDE provides a framework for pricing and analyzing exotic options, as the fractional derivative introduces additional flexibility to capture their unique characteristics.

(4) *Risk Management and Portfolio Optimization* The time-fractional Black–Scholes PDE can be used in risk management and portfolio optimization applications. By incorporating fractional derivatives, the model can account for long-range dependence and time-varying risk factors. This enables better estimation and management of risk in portfolios with assets that exhibit memory effects or non-Markovian behavior.

(5) *High-Frequency Trading and Market Microstructure* In high-frequency trading and market microstructure, the dynamics of financial markets at small timescales become crucial. The time-fractional Black–Scholes PDE can be used to model the price dynamics and option pricing in these fast-paced environments. The fractional derivative allows for capturing the intricate behavior of prices at small timescales, which is important for developing trading strategies and understanding market microstructure phenomena.

7 Conclusion

In this paper, an efficient collocation method based on exponential B-spline functions is introduced to solve the TFBSM governing European options. First, we have changed the modified R-L fractional derivative operator to the Caputo fractional derivative operator by applying the variable transformation, then used the exponential B-spline functions to discretize the space derivative and a finite difference method to discretize the Caputo fractional derivative. As a result of the use of the exponential B-spline collocation method, a tri-diagonal algebraic system has been obtained that can be solved by the Thomas algorithm. Furthermore, the proposed numerical scheme has been shown to be unconditionally stable via the von-Neumann method. Convergence analysis has also been provided for the proposed method. The method is implemented on a number of numerical examples. And the obtained results confirm that the method is capable of approximating the TFBSM. In addition, as an application, the numerical scheme proposed for the TFBSM has been used to price several different European options and it has been observed that the order of the time-fractional derivative has a great impact on the option prices. Since the proposed scheme works well for the TFBSM, so it is our intention to extend this idea to solve other fractional problems numerically.

Appendix A: Numerical Accuracy of Proposed Method

Example 2 Zhang et al. (2016a) We examine the problem (8)–(9) within the domain $(0, 1) \times (0, 1)$,

Table 2 (Example 2) L_∞ and L_2 errors with temporal order of convergence with $\rho = 1.5$ and $N_x = 200$

μ	N_t	L_∞-error	EOC	L_2-error	EOC	CPU time (s)
0.2	2^2	1.3142e−03		8.9644e−04		0.0511
	2^3	4.1644e−04	1.6580	2.8419e−04	1.6573	0.0588
	2^4	1.2878e−04	1.6932	8.7929e−05	1.6924	0.0979
	2^5	3.8884e−05	1.7277	2.6579e−05	1.7260	0.1763
	2^6	1.1273e−05	1.7863	7.7315e−06	1.7815	0.2943
0.4	2^2	3.7914e−03		2.5836e−03		0.0708
	2^3	1.3428e−03	1.4974	9.1567e−04	1.4965	0.1017
	2^4	4.6439e−04	1.5319	3.1682e−04	1.5312	0.2117
	2^5	1.5802e−04	1.5552	1.0786e−04	1.5545	0.1449
	2^6	5.2972e−05	1.5768	3.6187e−05	1.5756	0.3823
0.6	2^2	8.2022e−03		5.5778e−03		0.0770
	2^3	3.2827e−03	1.3211	2.2335e−03	1.3204	0.0840
	2^4	1.2846e−03	1.3536	8.7441e−04	1.3529	0.1099
	2^5	4.9605e−04	1.3727	3.3777e−04	1.3723	0.1599
	2^6	1.8988e−04	1.3854	1.2934e−04	1.3849	0.3154

Table 3 (Example 2) L_∞ and L_2 errors with spatial order of convergence with $\rho = 1.5$ and $N_t = 500$

μ	$N_\varkappa$	L_∞-error	EOC	L_2-error	EOC	CPU time (s)
0.2	2^2	2.3031e−03		1.3129e−03		0.4979
	2^3	5.4273e−04	2.0852	3.2284e−04	2.0239	0.3156
	2^4	1.3376e−04	2.0206	7.9810e−05	2.0162	0.3772
	2^5	3.3122e−05	2.0137	1.9753e−05	2.0145	0.3403
	2^6	8.0812e−06	2.0352	4.7919e−06	2.0434	0.4900
0.4	2^2	2.2197e−03		1.2661e−03		0.4334
	2^3	5.2005e−04	2.0936	3.0976e−04	2.0312	0.3363
	2^4	1.2692e−04	2.0348	7.5755e−05	2.0317	0.3693
	2^5	3.0408e−05	2.0614	1.7992e−05	2.0740	0.3902
	2^6	6.3578e−06	2.2579	3.6634e−06	2.2961	0.4647
0.6	2^2	2.1229e−03		1.2022e−03		0.3988
	2^3	4.8913e−0	2.1177	2.8985e−04	2.0524	0.3039
	2^4	1.1338e−04	2.1090	6.7110e−05	2.1107	0.3361
	2^5	2.2242e−05	2.3499	1.2686e−05	2.4033	0.3194
	2^6	5.2007e−06	2.0965	2.6649e−06	2.2511	0.4459

Table 4 (Example 2) Comparison with method in Akram et al. (2022) with $\mu = 0.6$, $N_\varkappa = 200$, and $N_t = 100$

$\varkappa$	$\widetilde{T} = 0.25$		$\widetilde{T} = 0.5$		$\widetilde{T} = 0.75$	
	Proposed method	Method in Akram et al. (2022)	Proposed method	Method in Akram et al. (2022)	Proposed method	Method in Akram et al. (2022)
0.1	2.947e−06	2.240e−05	7.424e−06	3.581e−05	1.444e−05	4.905e−05
0.2	3.889e−06	2.837e−05	1.201e−05	4.428e−05	2.504e−05	5.827e−05
0.3	4.161e−06	2.853e−05	1.563e−05	4.111e−05	3.423e−05	4.894e−05
0.4	4.119e−06	2.614e−05	1.845e−05	3.206e−05	4.181e−05	3.003e−03
0.5	3.708e−06	2.113e−05	1.990e−05	1.841e−05	4.636e−05	4.773e−06
0.6	2.753e−06	1.251e−05	1.919e−05	1.468e−07	4.618e−05	2.521e−05
0.7	1.158e−06	1.090e−07	1.573e−05	2.155e−05	3.979e−05	5.653e−05
0.8	8.348e−07	1.448e−05	9.688e−06	4.131e−05	2.737e−05	8.013e−03
0.9	2.164e−06	2.193e−05	2.825e−06	4.473e−05	1.157e−05	7.531e−05

$$ {}_0^C D_t^\mu u(\varkappa,t) = \alpha \frac{\partial^2 u(\varkappa,t)}{\partial \varkappa^2} + \beta \frac{\partial u(\varkappa,t)}{\partial \varkappa} - \gamma u(\varkappa,t) + \psi(\varkappa,t), $$

with

Table 5 (Example 2) L_∞-error and temporal order of convergence with $\alpha = 0.7$, $N_x = 150$ and $\rho = 1.5$

N_t	Present method			Method in [19]			Method in [14]	
	L_∞-error	EOC	CPU time (s)	L_∞-error	EOC	CPU time (s)	L_∞-error	EOC
10	3.6954e−03	–	0.0681	5.821e−03	–	0.0631	3.5000e−03	–
20	1.5349e−03	1.2676	0.0909	2.304e−03	1.3372	0.1272	1.4400e−03	1.3300
40	6.3094e−04	1.2825	0.1298	9.081e−04	1.3421	0.4075	5.9000e−04	1.3150
80	2.5756e−04	1.2926	0.3737	3.572e−04	1.3461	2.5240	2.4000e−04	1.3400
160	1.0443e−04	1.3024	0.3858	1.411e−04	1.3400	4.5321	9.5000e−05	1.3600
320	4.1888e−05	1.3179	0.8606	5.387e−05	1.3892	19.542	3.8000e−05	1.3800

Table 6 (Example 2) L_∞-error and spatial order of convergence with $\alpha = 0.7$, $N_t = 1000$ and $\rho = 1.5$

N_x	Present method		Method in [48]		Present method		Method in [48]	
	L_∞-error	EOC	L_∞-error	EOC	L_2-error	EOC	L_2-error	EOC
2^2	0.002	–	0.0030	–	0.001	–	0.0024	–
2^3	4.7739e−04	2.12	7.6750e−04	1.98	2.8144e−04	2.05	6.1678e−04	1.96
2^4	1.1112e−04	2.10	1.8629e−04	2.04	6.5497e−05	2.10	1.5079e−04	2.03
2^5	2.2337e−05	2.31	4.0698e−05	2.19	1.2680e−05	2.37	3.2995e−05	2.19

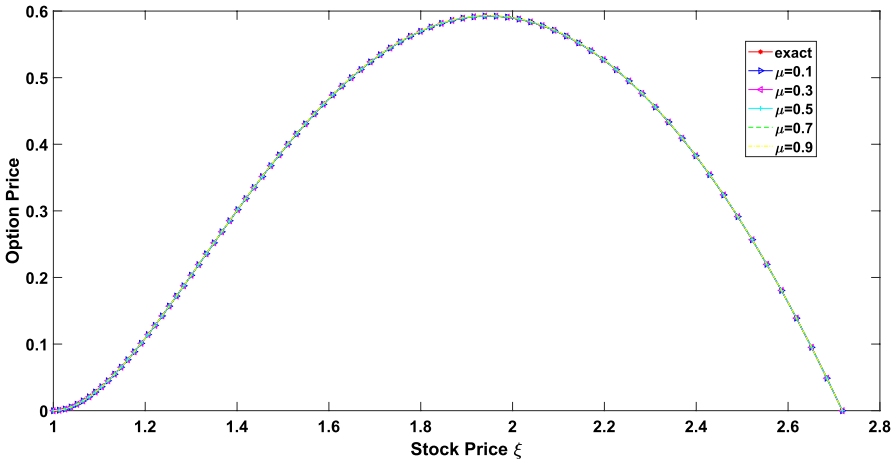

Fig. 9 Exact and numerical solutions of Example 2 with $\rho = 1.5$ and $N_x = N_t = 80$

$$\begin{cases} u(x,0) = x^2(1-x), \\ u(0,t) = 0, \\ u(1,t) = 0, \end{cases}$$

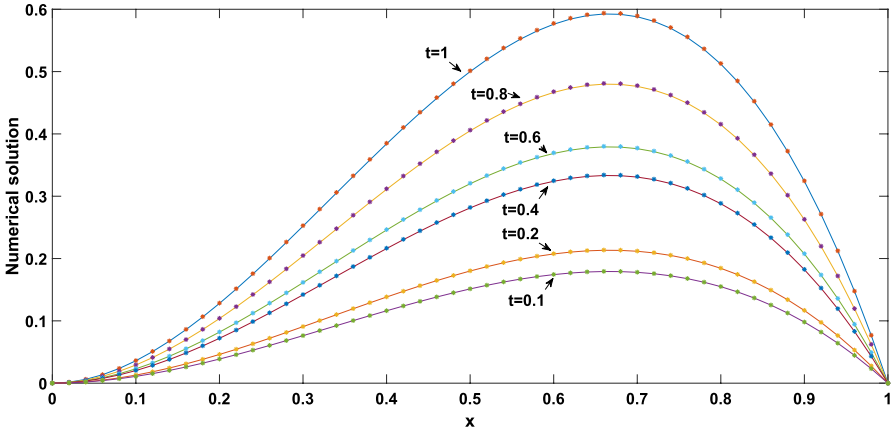

Fig. 10 Numerical solution (starred line) and exact solution (solid line) of Example 2 with $\mu = 0.9$, $\rho = 1.5$ and $N_x = N_t = 50$, at different time levels

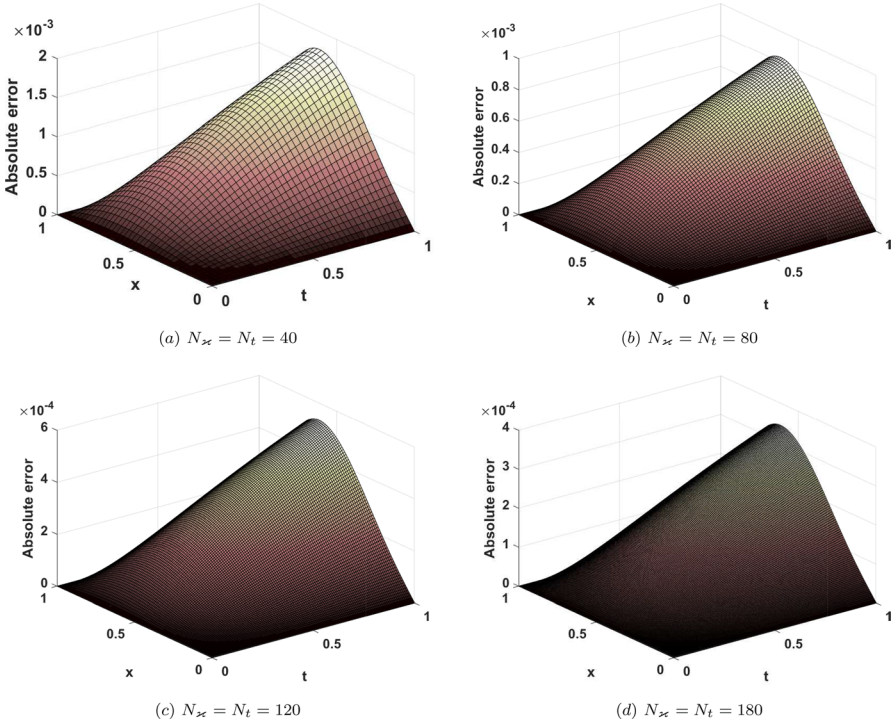

(a) $N_x = N_t = 40$ (b) $N_x = N_t = 80$

(c) $N_x = N_t = 120$ (d) $N_x = N_t = 180$

Fig. 11 Maximum absolute error plots for multiple N_x and N_t with $\mu = 0.9$ and $\rho = 1.5$ for Example 2

and the source term

$$\psi(x,t) = \frac{2}{\Gamma(3-\mu)}t^{2-\mu}x^2(1-x) + \frac{2}{\Gamma(2-\mu)}t^{1-\mu}x^2(1-x) - (t+1)^2(\alpha(2-6x) + \beta x(2-3x) - \gamma x^2(1-x)).$$

The exact solution of this test problem is $u(x,t) = (t+1)^2x^2(1-x)$. We will solve this problem with pre-mentioned values of parameters $r_f = 0.05, \sigma = 0.25$.

Table 2 contains L_∞ and L_2 errors together with temporal orders of convergence, for Example 2 with $\rho = 1.5$, $N_x = 200$, and different time spacings h_t for multiple values of μ. The outcomes displayed in this table substantiate the theoretical order of convergence derived in Theorem 4. Similarly, L_2 and L_∞ errors with corresponding spatial orders of convergence are calculated for $\rho = 1.5$, $N_t = 500$ and multiple values of μ, and are shown in Table 3. From this table, it can be viewed that as we increase the discretization points N_t, the errors decrease and the numerically calculated spatial order of convergence is 2, which is in support of the result proved in Theorem 4. In Table 4, we perform a comparison between our proposed exponential B-spline collocation method and the extended cubic B-spline collocation method introduced by Akram et al. (2022). Notably, our method demonstrates lower errors than Akram's approach for various time values $\widetilde{T}$. Moreover, Tables 5 and 6 provide a detailed comparison between our work and the studies conducted by Golbabai et al. (2019), De Staelen and Hendy (2017), and Zhang et al. (2016a) and lead to the conclusion that the numerical results demonstrate a strong correlation with these exiting methods. By visualizing the used CPU time for different temporal discretization steps, the scheme's

Table 7 (Example 3) L_∞ and L_2 errors with temporal order of convergence with $\rho = 0.5$ and $N_x = 1000$

μ	N_t	L_∞-error	EOC	L_2-error	EOC	CPU time (s)
0.2	2^2	2.0501e−03		1.4973e−03		1.0925
	2^3	6.4353e−04	1.6716	4.6999e−04	1.6717	2.3466
	2^4	1.9850e−04	1.6968	1.4497e−04	1.6969	3.8748
	2^5	6.0452e−05	1.7153	4.4148e−05	1.7153	8.1613
	2^6	1.8246e−05	1.7282	1.3325e−05	1.7282	17.481
0.4	2^2	5.8311e−03		4.2575e−03		1.1709
	2^3	2.0210e−03	1.5287	1.4755e−03	1.5288	2.2319
	2^4	6.9083e−04	1.5487	5.0435e−04	1.5487	4.2051
	2^5	2.3392e−04	1.5623	1.7077e−04	1.5624	9.4313
	2^6	7.8691e−05	1.5717	5.7447e−05	1.5718	26.125
0.6	2^2	1.2591e−02		9.1890e−03		1.2219
	2^3	4.8905e−03	1.3643	3.5690e−03	1.3644	2.0352
	2^4	1.8821e−03	1.3777	1.3734e−03	1.3777	3.8258
	2^5	7.2030e−04	1.3856	5.2562e−04	1.3857	8.6898
	2^6	2.7473e−04	1.3906	2.0048e−04	1.3906	14.883

Table 8 (Example 3) L_∞ and L_2 errors with spatial order of convergence with $\rho = 0.5$ and $N_t = 2500$

μ	N_x	L_∞-error	EOC	L_2-error	EOC	CPU time (s)
0.2	2^2	2.7740e−03		2.0482e−03		8.0030
	2^3	6.9807e−04	1.9905	5.1071e−04	2.0037	8.5853
	2^4	1.7615e−04	1.9866	1.2755e−04	2.0015	14.000
	2^5	4.4043e−05	1.9998	3.1892e−05	1.9998	36.208
	2^6	1.1038e−05	1.9965	7.9881e−06	1.9973	221.05
0.4	2^2	2.7661e−03		2.0425e−03		7.7701
	2^3	6.9623e−04	1.9902	5.0936e−04	2.0036	8.6705
	2^4	1.7582e−04	1.9855	1.2732e−04	2.0003	13.971
	2^5	4.4114e−05	1.9948	3.1946e−05	1.9947	40.564
	2^6	1.1209e−05	1.9765	8.1137e−06	1.9772	222.86
0.6	2^2	2.7643e−03		2.0413e−03		7.5126
	2^3	6.9683e−04	1.9880	5.0980e−04	2.0015	8.6314
	2^4	1.7701e−04	1.9770	1.2819e−04	1.9916	14.082
	2^5	4.5467e−05	1.9610	3.2936e−05	1.9606	38.529
	2^6	1.2603e−05	1.8510	9.1312e−06	1.8508	200.23

Table 9 (Example 3) L_∞-error and temporal order of convergence with $\alpha = 0.7$, $N_x = 100$ and $\rho = 0.5$

N_t	Present method			Method in [1]		Method in [48]	
	L_∞-error	EOC	CPU time (s)	L_∞-error	EOC	L_∞-error	EOC
10	5.4839e−03		0.0780	1.18093e−03		0.0055	
20	2.2477e−03	1.2867	0.0502	4.76255e−04	1.3101	0.0022	1.3219
40	9.1989e−04	1.2889	0.1062	1.89732e−04	1.3277	8.9427e−04	1.2987
80	3.7734e−04	1.2856	0.1674	7.45705e−05	1.3472	3.5176e−04	1.3461
160	1.5618e−04	1.2726	0.2873	2.99343e−05	1.3168	1.3065e−04	1.4289

Table 10 (Example 3) L_∞-error and spatial order of convergence with $\alpha = 0.7$, $N_t = 1000$ and $\rho = 0.5$

N_x	Present method		Method in [48]		Present method		Method in [48]	
	L_∞-error	EOC	L_∞-error	EOC	L_2-error	EOC	L_2-error	EOC
2^2	2.7773e−03		0.0132		2.0510e−03		0.0024	
2^3	7.0932e−04	1.9692	0.0033	2.0000	5.1899e−04	1.9825	6.1678e−04	1.9602
2^4	1.8944e−04	1.9047	8.1906e−04	2.0104	1.3727e−04	1.9187	1.5079e−04	2.0322
2^5	4.7860e−05	1.9848	1.9457e−04	2.0737	3.4748e−05	1.9820	3.2995e−05	2.1922

proficiency in delivering accurate results while maintaining minimal CPU usage becomes evident. Figs. 9 and 12 represent the exact and numerical solutions taking different fractional orders μ for Examples 2 and 3 respectively. From these graphs, we can say that the proposed method approximates the TFBSM very

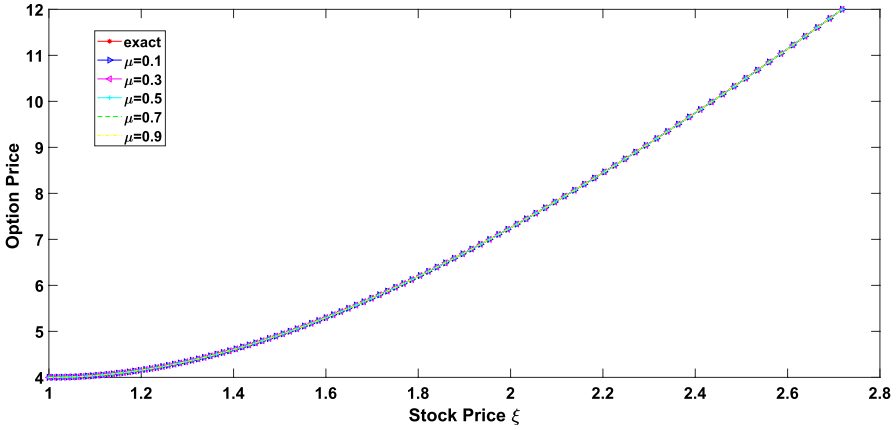

Fig. 12 The exact and numerical solutions of Example 3 with $\rho = 0.5$ and $N_x = N_t = 100$

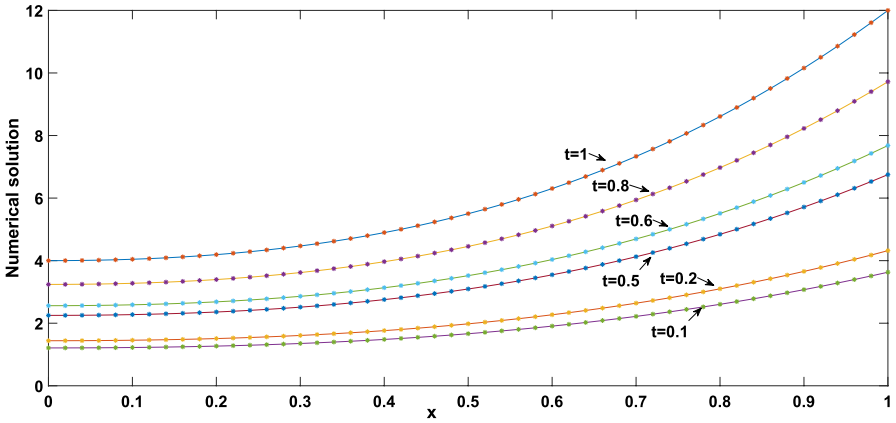

Fig. 13 The numerical solution (starred line) and the exact solution (solid line) of Example 3 with $\mu = 0.9$, $\rho = 0.5$ and $N_x = N_t = 50$, at different time t

well. At different time levels, the graphs displayed in Figs. 10 and 13 illustrate the comparison between the exact and numerical solutions of Examples 2 and 3, respectively. Upon examining these graphs, it becomes evident that the exact and numerical solutions exhibit nearly identical behavior. Moreover, Fig. 11 presents three-dimensional graphics depicting the maximum errors for Example 2 with $\rho = 1.5$, $\mu = 0.9$, and different combinations of N_x and N_t.

Example 3 We examine the problem (8)–(9) within the domain $(0,1)\times(0,1)$,

$$ {}_0^C D_t^{\mu} u(\varkappa,t) = \alpha \frac{\partial^2 u(\varkappa,t)}{\partial \varkappa^2} + \beta \frac{\partial u(\varkappa,t)}{\partial \varkappa} - \gamma u(\varkappa,t) + \psi(\varkappa,t), $$

with

$$ \begin{cases} u(\varkappa,0) = 1+\varkappa^2+\varkappa^3, \\ u(0,t) = (1+t)^2, \\ u(1,t) = 3(1+t)^2, \end{cases} $$

and the source term

$$ \begin{aligned} \psi(\varkappa,t) = &\left(\frac{2t^{2-\mu}}{\Gamma(3-\mu)} + \frac{2t^{1-\mu}}{\Gamma(2-\mu)} \right)(1+\varkappa^2+\varkappa^3) \\ &- (t+1)^2\big(\alpha(6\varkappa+2) + \beta\varkappa(2+3\varkappa) - \gamma(1+\varkappa^2+\varkappa^3)\big). \end{aligned} $$

The exact solution of this test problem is $u(\varkappa,t) = (t+1)^2(1+\varkappa^2+\varkappa^3)$. We will solve this problem with pre-mentioned values of parameters $r_f = 0.5$, $\alpha = 1$.

The numerical results obtained by applying the proposed method for Example 3 are given in Tables 7, 8, 9, and 10. Table 7, gives the errors L_∞ and L_2 with the corresponding temporal orders of convergence calculated for $\rho = 0.5$, $N_\varkappa = 1000$, and different fractional orders μ. By examining the values in this table, we can deduce that the numerically determined temporal order of convergence is approximately $2-\mu$. Similarly, from Table 8, we can see that the spatial order of convergence is two obtained for multiple fractional orders μ using $\rho = 0.5$, $N_t = 2500$. In addition, Tables 9 and 10 provide a detailed comparison between our work and the studies conducted by Akram et al. (2022) and Zhang et al. (2016a) and lead to the conclusion that the numerical results are in good agreement with these exiting methods. Also, the CPU time for different temporal discretization steps has been provided. The scheme not only provides highly accurate results but also achieves this with remarkably low CPU time consumption.

Example 4 Kadalbajoo et al. (2012) Considering the European call option governed by the classical Black–Scholes Eq. (1), we adopt the following parameter values: $\sigma = 0.4$, $r_f = 0.06$, $D_Y = 0.02$, and $\widetilde{T} = 1$. In this particular case, where the Black–Scholes equation incorporates the final condition $\mathcal{V}(\xi,\widetilde{T}) = \max(\xi-\widetilde{K},0)$ and the boundary conditions $\mathcal{V}(0,\tau) = 0$ and $\mathcal{V}(\xi,\tau) = \xi\exp(-D_Y(\widetilde{T}-\tau)) - \widetilde{K}\exp(-r_f(\widetilde{T}-\tau))$ as $\xi\to\infty$, the exact solution is expressed as

$$ \mathcal{V}(\xi,\tau) = \xi\mathcal{Y}(\mathcal{C}_1)\exp(-D_Y(\widetilde{T}-\tau)) - \widetilde{K}\mathcal{Y}(\mathcal{C}_2)\exp(-r_f(\widetilde{T}-\tau)), \tag{62} $$

where

Table 11 (Example 4) Comparison with method in Kadalbajoo et al. (2012)

$N_x = N_t$	Proposed method		Method in Kadalbajoo et al. (2012)	
	L_2-error	EOC	L_2-error	EOC
10	1.461976e−02	–	1.527893e−02	–
20	5.621419e−03	1.3789	5.716950e−03	1.4182
40	2.074532e−03	1.4381	2.087466e−03	1.4534
80	7.987847e−04	1.3769	8.004962e−04	1.3827
160	3.487558e−04	1.1955	3.489781e−04	1.1977

$$\mathcal{Y}(\varkappa) = \frac{1}{\sqrt{2\pi}} \int_{-\infty}^{\varkappa} \exp\left(-\omega^2/2\right) d\omega,$$

$$\mathcal{C}_1(\xi,\tau) = \frac{\ln\left(\frac{\xi}{\widetilde{K}}\right) + \left(r_f - D_Y + \frac{\sigma^2}{2}\right)(\widetilde{T}-\tau)}{\sigma\sqrt{(\widetilde{T}-\tau)}}, \text{ and } \mathcal{C}_2(\xi,\tau) = \mathcal{C}_1(\xi,\tau) - \sigma\sqrt{(\widetilde{T}-\tau)}.$$

Moving forward, we adopt an approximation strategy (Cen and Le 2011; Kadalbajoo et al. 2012) to represent the final condition $\max(\xi - \widetilde{K}, 0)$ using a suitably smooth function $\phi(\xi) = \mathcal{D}(\xi - \widetilde{K})$, where

$$\mathcal{D}(\omega) = \begin{cases} \omega, & \text{if } \omega \geq \varepsilon, \\ a_0 + a_1\omega + a_2\omega^2 \cdots + a_9\omega^9, & \text{if } -\varepsilon < \omega < \varepsilon, \\ 0, & \text{if } \omega \leq \varepsilon, \end{cases}$$

for sufficiently small $\varepsilon > 0$. Here by using ten conditions $\mathcal{D}(-\varepsilon) = \mathcal{D}'(-\varepsilon) = \mathcal{D}''(-\varepsilon) = \mathcal{D}'''(-\varepsilon) = \mathcal{D}^{(4)}(-\varepsilon) = 0, \mathcal{D}(\varepsilon) = \varepsilon, \mathcal{D}'(\varepsilon) = 1, \mathcal{D}''(\varepsilon) = \mathcal{D}'''(\varepsilon) = \mathcal{D}^{(4)}(\varepsilon) = 0$, we can obtain

$$a_0 = \frac{35\varepsilon}{256},\ a_1 = \frac{1}{2},\ a_2 = \frac{3}{64\varepsilon},\ a_4 = \frac{-35}{128\varepsilon^3},$$
$$a_6 = \frac{7}{64\varepsilon^5},\ a_8 = \frac{-5}{256\varepsilon^7},\ a_3 = a_5 = a_7 = a_9 = 0.$$

Consequently, through the utilization of the aforementioned approximation and introducing the transformations $\xi = \exp(\varkappa)$ and $t = \widetilde{T} - \tau$, the original Black–Scholes equation, initially degenerate and backward in time, undergoes a transformation into a non-degenerate and forward in time partial differential equation. This transformation also yields a smooth initial condition for the equation

$$\frac{\partial u}{\partial t} = \alpha\frac{\partial^2 u}{\partial \varkappa^2} + \beta\frac{\partial u}{\partial \varkappa} - \gamma u, \quad (\varkappa, t) \in (I_p, F_p) \times (0, \widetilde{T}),$$

with

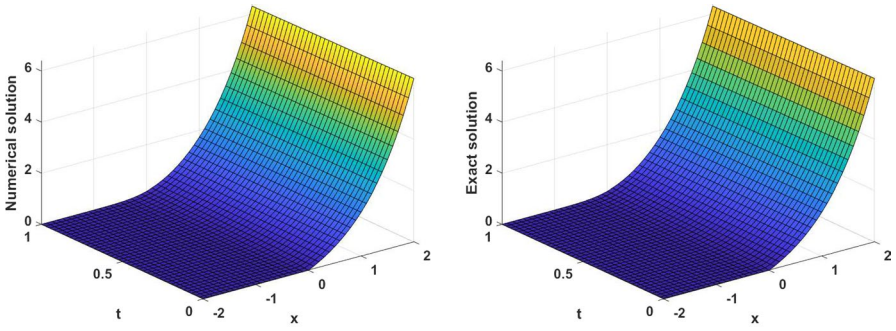

(a) Numerical solution (b) Exact solution

Fig. 14 Three dimension graphics of solutions of Example 4 with $\mu = 1$, $\rho = 2$, $N_x = N_t = 40$, and $\varepsilon = 10^{-6}$

$$\begin{cases} u(x,0) = z_0(x), \\ u(I_p,t) = 0, \\ u(F_p,t) = \exp(F_p - D_Y t) - \widetilde{K}\exp(-r_f t), \end{cases}$$

where $u(x,t) = \mathcal{V}(\exp(x), \widetilde{T} - t)$, $z_0(x) = \phi(\exp(x))$, $\alpha = 0.08$, $\beta = -0.04$ and $\gamma = 0.06$. The transformed exact solution is

$$u(x,t) = \mathcal{Y}(\mathcal{C}_1)\exp(x - D_Y t) - \widetilde{K}\mathcal{Y}(\mathcal{C}_2)\exp(-r_f t), \tag{63}$$

where

$$\mathcal{C}_1(x,t) = \frac{x - \ln\left(\widetilde{K}\right) + \left(r_f - D_Y + \frac{\sigma^2}{2}\right)t}{\sigma\sqrt{t}}, \text{ and } \mathcal{C}_2(x,t) = \mathcal{C}_1(x,t) - \sigma\sqrt{t}.$$

For computational purposes, we adopt the assumptions $I_p = -2$, $F_p = +2$, and $\varepsilon = 10^{-6}$.

The motivation behind considering this problem is to demonstrate the capability of our proposed method to handle the classical Black–Scholes PDE with remarkable accuracy, just as it does for the fractional version. In Table 11, we have provided the L_2-error values along with the corresponding numerical order of convergence while keeping $\mu = 1$ fixed. Besides, this table provides a comparison between our method and the cubic spline collocation method proposed in Kadalbajoo et al. (2012). The numerical results highlight a robust correlation between our method and the existing approach, demonstrating that our method is equally effective in handling the classical Black–Scholes PDE. Furthermore, for $\mu = 1$, $\rho = 2$, $N_x = N_t = 40$, and $\varepsilon = 10^{-6}$, Fig. 14 presents the three-dimensional representations of the numerical and exact solutions. Notably, the graphics

demonstrate a remarkable similarity, indicating a high level of agreement between the two solutions.

Acknowledgements The authors would like to express great appreciation to anonymous reviewers for their valuable comments and suggestions, which have helped to improve the quality and presentation of this paper. A preprint of this paper is available on arxiv with Ref. No. arXiv:2207.09153

Author Contributions All authors contributed equally. All authors read and approved the final manuscript.

Funding The authors declare that no funds, grants, or other support were received during the preparation of this manuscript.

Declarations

Conflict of interest The authors have no relevant financial or non-financial interests to disclose.

References

Akram, T., Abbas, M., Abualnaja, K. M., Iqbal, A., & Majeed, A. (2022). An efficient numerical technique based on the extended cubic B-spline functions for solving time fractional Black–Scholes model. *Engineering with Computers, 38*(2), 1705–1716.

Amster, P., Averbuj, C., & Mariani, M. (2002). Solutions to a stationary nonlinear Black–Scholes type equation. *Journal of Mathematical Analysis and Applications, 276*(1), 231–238.

Amster, P., Averbuj, C., & Mariani, M. (2003). Stationary solutions for two nonlinear Black–Scholes type equations. *Applied Numerical Mathematics, 47*(3–4), 275–280.

An, X., Liu, F., Zheng, M., Anh, V. V., & Turner, I. W. (2021). A space-time spectral method for time-fractional Black–Scholes equation. *Applied Numerical Mathematics, 165*, 152–166.

Black, F., Scuholes, M. The pricing of options and corporate liabilities. In: World Scientific Reference on Contingent Claims Analysis in Corporate Finance: Volume 1: Foundations of CCA and Equity Valuation, pp. 3–21. World Scientific (2019)

Bohner, M., & Zheng, Y. (2009). On analytical solutions of the Black–Scholes equation. *Applied Mathematics Letters, 22*(3), 309–313.

Carr, P., & Wu, L. (2003). The finite moment log stable process and option pricing. *The Journal of Finance, 58*(2), 753–777.

Cartea, A., & Del-Castillo-Negrete, D. (2007). Fractional diffusion models of option prices in markets with jumps. *Physica A: Statistical Mechanics and its Applications, 374*(2), 749–763.

Cen, Z., & Le, A. (2011). A robust and accurate finite difference method for a generalized Black–Scholes equation. *Journal of Computational and Applied Mathematics, 235*(13), 3728–3733.

Chen, W., Xu, X., & Zhu, S. P. (2015). Analytically pricing double barrier options based on a time-fractional Black–Scholes equation. *Computers & Mathematics with Applications, 69*(12), 1407–1419.

Company, R., Jódar, L., & Pintos, J. R. (2009). A numerical method for European Option Pricing with transaction costs nonlinear equation. *Mathematical and Computer Modelling, 50*(5–6), 910–920.

Company, R., Navarro, E., Pintos, J. R., & Ponsoda, E. (2008). Numerical solution of linear and nonlinear Black–Scholes option pricing equations. *Computers & Mathematics with Applications, 56*(3), 813–821.

De Boor, C., & De Boor, C. (1978). *A practical guide to splines* (Vol. 27). New York: Springer-Verlag.

De Staelen, R. H., & Hendy, A. S. (2017). Numerically pricing double barrier options in a time-fractional Black–Scholes model. *Computers & Mathematics with Applications, 74*(6), 1166–1175.

Edeki, S. O., Ugbebor, O. O., & Owoloko, E. A. (2017). Analytical solution of the time-fractional order Black–Scholes model for stock option valuation on no dividend yield basis. *IAENG International Journal of Applied Mathematics, 47*(4), 1–10.

Fall, A. N., Ndiaye, S. N., & Sene, N. (2019). Black–Scholes option pricing equations described by the Caputo generalized fractional derivative. *Chaos, Solitons & Fractals, 125*, 108–118.

Ghandehari, M., & Ranjbar, M. (2014). European option pricing of fractional version of the Black–Scholes model: Approach via expansion in series. *International Journal of Nonlinear Science, 17*(2), 105–110.

Golbabai, A., & Mohebianfar, E. (2017). A new stable local radial basis function approach for option pricing. *Computational Economics, 49*(2), 271–288.

Golbabai, A., Nikan, O., & Nikazad, T. (2019). Numerical analysis of time fractional Black–Scholes European option pricing model arising in financial market. *Computational and Applied Mathematics, 38*, 1–24.

Gupta, V., & Kadalbajoo, M. K. (2016). Qualitative analysis and numerical solution of burgers' equation via b-spline collocation with implicit Euler method on piecewise uniform mesh. *Journal of Numerical Mathematics, 24*(2), 73–94.

Hariharan, G., Padma, S., & Pirabaharan, P. (2013). An efficient wavelet based approximation method to time-fractional Black–Scholes European option pricing problem arising in financial market. *Applied Mathematical Sciences, 7*(69), 3445–3456.

Jumarie, G. (2008). Stock exchange fractional dynamics defined as fractional exponential growth driven by (usual) Gaussian white noise. Application to fractional Black–Scholes equations. *Insurance Mathematics and Economics, 42*(1), 271–287.

Jumarie, G. (2010). Derivation and solutions of some fractional Black–Scholes equations in coarse-grained space and time. Application to Merton's optimal portfolio. *Computers & Mathematics with Applications, 59*(3), 1142–1164.

Kadalbajoo, M. K., Gupta, V., & Awasthi, A. (2008). A uniformly convergent b-spline collocation method on a nonuniform mesh for singularly perturbed one-dimensional time-dependent linear convection-diffusion problem. *Journal of Computational and Applied Mathematics, 220*(1), 271–289.

Kadalbajoo, M. K., & Gupta, V. (2009). Numerical solution of singularly perturbed convection-diffusion problem using parameter uniform b-spline collocation method. *Journal of Mathematical Analysis and Applications, 355*(1), 439–452.

Kadalbajoo, M. K., & Gupta, V. (2010). A parameter uniform b-spline collocation method for solving singularly perturbed turning point problem having twin boundary layers. *International Journal of Computer Mathematics, 87*(14), 3218–3235.

Kadalbajoo, M. K., Tripathi, L. P., & Kumar, A. (2012). A cubic B-spline collocation method for a numerical solution of the generalized Black–Scholes equation. *Mathematical and Computer Modelling, 55*(3–4), 1483–1505.

Koleva, M. N., & Vulkov, L. G. (2017). Numerical solution of time-fractional Black–Scholes equation. *Computational and Applied Mathematics, 36*(4), 1699–1715.

Li, C., & Zeng, F. (2019). *Numerical methods for fractional calculus*. Chapman and Hall/CRC.

Liang, J. R., Wang, J., Zhang, W. J., Qiu, W. Y., & Ren, F. Y. (2010). Option pricing of a bi-fractional Black-Merton-Scholes model with the Hurst exponent H in [12, 1]. *Applied Mathematics Letters, 23*(8), 859–863.

McCartin, B. J. (1991). Theory of exponential splines. *Journal of Approximation Theory, 66*(1), 1–23.

Merton, R. C. (1973). Theory of rational option pricing. *The Bell Journal of Economics and Management Science, 1973*, 141–183.

Mesgarani, H., Beiranvand, A., & Aghdam, Y. E. (2021). The impact of the Chebyshev collocation method on solutions of the time-fractional Black–Scholes. *Mathematical Sciences, 15*(2), 137–143.

Podlubny, I. (1998). *Fractional differential equations: an introduction to fractional derivatives, fractional differential equations, to methods of their solution and some of their applications*. Elsevier.

Prathumwan, D., & Trachoo, K. (2020). On the solution of two-dimensional fractional Black–Scholes equation for European put option. *Advances in Difference Equations, 2020*(1), 1–9.

Pruess, S. (1976). Properties of splines in tension. *Journal of Approximation Theory, 17*(1), 86–96.

Pruess, S. (1979). Alternatives to the exponential spline in tension. *Mathematics of Computation, 33*(148), 1273–1281.

Rao, S. C. S., & Kumar, M. (2008). Exponential b-spline collocation method for self-adjoint singularly perturbed boundary value problems. *Applied Numerical Mathematics, 58*(10), 1572–1581.

Rao, S. C. S., Kumar, S., & Kumar, M. (2010). A parameter-uniform b-spline collocation method for singularly perturbed semilinear reaction-diffusion problems. *Journal of Optimization Theory and Applications, 146*, 795–809.

Ravi Kanth, A. S. V., & Garg, N. (2021). An unconditionally stable algorithm for multiterm time fractional advection-diffusion equation with variable coefficients and convergence analysis. *Numerical Methods for Partial Differential Equations, 37*(3), 1928–1945.

Ravi Kanth, A. S. V., & Garg, N. (2022). A computational procedure and analysis for multi-term time-fractional burgers-type equation. *Mathematical Methods in the Applied Sciences, 45*(16), 9218–9232.

Rodrigo, M. R., & Mamon, R. S. (2006). An alternative approach to solving the Black–Scholes equation with time-varying parameters. *Applied Mathematics Letters, 19*(4), 398–402.

Singh, A., & Kumar, S. (2023). A convergent exponential B-spline collocation method for a time-fractional telegraph equation. *Computational and Applied Mathematics, 42*(2), 79.

Singh, A., Kumar, S., & Vigo-Aguiar, J. (2023). A fully discrete scheme based on cubic splines and its analysis for time-fractional reaction-diffusion equations exhibiting weak initial singularity. *Journal of Computational and Applied Mathematics, 434*, 115338.

Singh, A., Kumar, S., & Vigo-Aguiar, J. (2023). *High-order schemes and their error analysis for generalized variable coefficients fractional reaction-diffusion equations Mathematical Methods in the Applied Sciences*. Wiley Online Library.

Song, L., & Wang, W. (2013). Solution of the fractional Black–Scholes option pricing model by finite difference method. *Abstract and Applied Analysis, 2013*, 1–10.

Wyss, Walter. (2000). The fractional Black–Scholes equation. *Fractional Calculus and Applied Analysis, 1*, 51–61.

Zhang, H., Liu, F., Turner, I., & Yang, Q. (2016). Numerical solution of the time-fractional Black–Scholes model governing European options. *Computers & Mathematics with Applications, 71*(9), 1772–1783.

Zhang, H. M., Liu, F. W., Turner, I., & Chen, S. (2016). The numerical simulation of the tempered fractional Black–Scholes equation for European double barrier option. *Applied Mathematical Modelling, 40*(11–12), 5819–5834.